DISSERTATION

Investigation and modelling of voltage-current-, voltage-magnetic field-, and voltage-temperature-characteristics of different superconductors

ausgeführt zum Zwecke der Erlangung des akademischen Grades eines Doktors der technischen Wissenschaften

unter der Leitung von

em. o. Prof. Dipl.-Ing. Dr. techn. Hans R. KIRCHMAYR,
Institut für Festkörperphysik (E138),

eingereicht an der Technischen Universität Wien,
Fakultät für Physik,

von

Dipl.-Ing. Martin MÜLLER
Matrikelnummer: 9425393
1100 WIEN, Karmarschgasse 51/2/45

Wien, im Mai 2004

Dipl.-Ing. Martin Müller

Deutsche Kurzfassung

Die vorliegende Dissertation behandelt die Untersuchung von Spannungs-Strom-, Spannungs-Magnetfeld- und Spannungs-Temperatur-Charakteristiken dreier verschiedener supraleitender Materialien: das erste ist ein technischer Tieftemperatursupraleiter, Nb_3Sn, das zweite ein technischer Hochtemperatursupraleiter, $Bi_2Sr_2Ca_2Cu_3O_{10}$ (Bi-2223), und das dritte ein klassischer Typ-I-Supraleiter, nämlich Blei (Pb).

Im Rahmen eines Optimierungs- und Prüfungsprogrammes von multifilamentären Nb_3Sn-Drähten wurde beim Auswerten gemessener Spannungs-Strom-Charakteristiken festgestellt, daß der Übergang vom supraleitenden in den normalleitenden Zustand durch ein Potenzgesetz der Form $U(I) = k_{(\mathrm{I})} I^n$ beschrieben werden kann, wobei der Exponent n eine Funktion des kritischen Stromes ist.

Die Optimierung von Nb_3Sn-Supraleitern wurde im Hinblick auf den geplanten Bau des thermonuklearen Fusionsreaktors ITER durchgeführt, um möglichst hohe kritische Stromdichten bei gleichzeitig akzeptablen Restwiderstandsverhältnis (RRR) und Hystereseverlusten zu erzielen. Optimiert wurden das Drahtdesign und die Produktionsprozesse, aber auch die Wärmebehandlung der Drähte, die nötig ist, um den Supraleiter zu bilden.

Das erste Kapitel soll die Ideen darlegen, die hinter dem Bau des ITER stehen. Weiters werden die felderzeugenden Spulen beschrieben und die Materialien, aus denen sie hergestellt werden sollen.

Im zweiten Kapitel finden sich die wichtigsten Informationen über den Aufbau und die technischen Eigenschaften der untersuchten Nb_3Sn-Drähte, gefolgt von einer detaillierten Diskussion der Optimierung des Wärmebehand-

lungsprozesses und seiner Ergebnisse. Aufgrund der Tatsache, daß verschiedene Hersteller Drähte für ITER produzieren, ist es von besonderem Interesse, einen vereinheitlichten Wärmebehandlungszyklus zu finden, dem verschiedene Drahttypen gleichzeitig unterzogen werden können. Der letzte Schritt dieser Vereinheitlichung wurde im Rahmen dieser Arbeit getan.

Kapitel drei behandelt die Details betreffend die Probenpräparation, das Meßsystem und die Durchführung von Spannungs-Strom-, Spannungs-Magnetfeld- und Spannungs-Temperatur-Messungen. Es sei betont, daß Spannungs-Magnetfeld- und Spannungs-Temperatur-Messungen auf dem Institut für Festkörperphysik erstmals durchgeführt worden sind.

Nach einem kurzen Rückblick auf die Ergebnisse früherer Spannungs-Strom-Messungen und das Skalierungsverhalten des Exponenten n als Funktion des kritischen Stromes, welches für Nb_3Sn gefunden wurde, wird in Kapitel vier gezeigt, daß ein Skalierungsgesetz von $n(I_c)$ auch für Bi-2223 und Blei existiert. Darüberhinaus wird für Nb_3Sn, Bi-2223 und Blei gezeigt, daß auch die gemessenen Spannungs-Magnetfeld- und Spannungs-Temperatur-Kurven durch ein Potenzgesetz, ähnlich zu obigem, angepaßt werden können und daß die Exponenten o und m ebenfalls Funktionen der zugehörigen kritischen Größen B_c und T_c sind.

Schließlich wird im fünften Kapitel die Entwicklung eines mathematischen Modells zur Berechnung von Spannungs-Strom-, Spannungs-Magnetfeld- und Spannungs-Temperatur-Charakteristiken von Nb_3Sn beschrieben. Es wird durch Vergleich mit den aus Messungen gewonnenen Daten gezeigt werden, daß das Modell in der Lage ist, diese Charakteristiken und auch das Skalierungsverhalten seiner Exponenten richtig vorherzusagen.

Acknowledgement

First of all I have to thank my supervisor, o. Prof. Dr. Hans Kirchmayr, for giving me a very interesting task and the opportunity of making this doctoral thesis. I am also very grateful for his mental support and that lot of scientific discussions he was always open for.

A great deal of thanks I have to express to my co-assessor, Prof. Dr. Günter Wiesinger, for giving me a lot of advice during my work on this thesis and for carefully reading through and correcting the text.

My thanks have to be extended to Dr. Klaus Hense, who encouraged me to try to develop the mathematical model, and to my co-worker Harald Schulz, who helped me a lot with the measurements.

Additionally, I would like to thank the team of the institute's workshop for always being helpful and quickly solving my technical problems by supplying me with their experience.

Finally I have to express my gratitude to all members of the former Institute of Experimental Physics for the exceedingly pleasant working atmosphere and for their continuous and unresting assistance with both professional and personal concerns.

Contents

Outline

This dissertation deals with the investigation of voltage-current-, voltage-magnetic field-, and voltage-temperature-characteristics of three different superconducting materials: the first a technological low-T_c-superconductor, Nb_3Sn, the second a technological high-T_c-superconductor, $Bi_2Sr_2Ca_2Cu_3O_{10}$ (Bi-2223), and the third a classical type-I-superconductor, lead (Pb).

Within an optimisation and testing programme, by evaluating measured voltage-current-characteristics of multifilamentary Nb_3Sn strands it was found that the transition from the superconducting to the normally conducting state can be described using a power law of the form $U(I) = k_{(\mathrm{I})} I^n$, where the exponent n is a function of critical current.

The optimisation of Nb_3Sn-type superconductors has been carried out with respect to highest possible critical current densities and acceptable values of the residual resistance ratio (RRR) and hysteresis losses, respectively, in the face of the intended build-up of an experimental thermonuclear fusion reactor, called ITER. Optimised have been the strands' designs and production processes as well as the heat treatment of the strands, which is necessary to form the superconductor.

The first chapter of this thesis gives an introduction into the ideas behind ITER. It is described how the magnetic field generating coils will be designed and which superconducting materials will be used for manufacturing those coils. The introduction ends with a description of the European Fusion Development Agreement (EFDA), since this organisation coordinates many working groups, which are spread all over Europe. One of those groups, which the author is member of, is located in the Institute of Solid State

Physics at Vienna University of Technology.

The second chapter is giving detailed information on the layout and performance parameters of the investigated Nb_3Sn strands, followed by a detailed discussion of the optimisation of the heat treatment process and its results. As until recently there were only two strand manufacturers in Europe (Europa Metalli and Vacuumschmelze) and at the moment there exist six producers providing strands for the ITER coils, it is of particular interest to find a unified heat treatment cycle, which different strand types can be undergone at the same time. The last step of such a unification was done within the scope of this work and is therefore described here.

Chapter three treats all details which are noteworthy for understanding of how the measurement data are obtained. After a short introduction into the skills of sample preparation and the main components of the measuring system it is described in detail, how voltage-current-, voltage-magnetic field-, and voltage-temperature measurements are carried out. It is important to mention that voltage-magnetic field-, as well as voltage-temperature-curves have been measured in the Institute of Solid State Physics for the first time.

After a short review of the results of earlier voltage-current-measurements and the scaling behaviour of the exponent n as a function of critical current found for Nb_3Sn, it will be shown in chapter four that a scaling law of $n(I_c)$ can also be found for Bi-2223 and lead. Furthermore, it is shown that the measured voltage-magnetic field- and voltage-temperature-curves can also be fitted using a power law similar to that given above and that the exponents o and m are functions of the associated critical parameters B_c and T_c. This is done for Nb_3Sn, Bi-2223, and lead.

Finally, in chapter five the development of a mathematical model for the calculation of voltage-current-, voltage-magnetic field-, and voltage-temperature-characteristics of Nb_3Sn is described. It will be shown that this model is capable of predicting those characteristics and the scaling behaviour of their exponents. Calculated and measured data are compared to each other and a good agreement of both is asserted.

1 Introduction

1.1 What is ITER?

The International Thermonuclear Experimental Reactor (ITER) is an international collaborative project undertaken jointly by the world's leading fusion energy programmes with the objective of demonstrating the scientific and technological feasability of fusion energy for peaceful purposes. To do this, ITER will demonstrate moderate power multiplication, demonstrate essential fusion energy technologies in a system integrating the appropriate physics and technology, and test key elements required to use fusion as a practical energy source. It will be the first fusion device to produce thermal energy at the level of an electricity-producing power station. Furthermore, it will provide the next major step for the advancement of fusion science and technology, and is anticipated to be the key element in the strategy to reach the following demonstration electricity-generating power plant in a single experimental step.

The initial members of the ITER project were Euratom, Japan, the Russian Federation, Canada, and the United States of America. In February 2003 they were joined by the People's Republic of China and again by the United States of America and in May 2003 by the Republic of Korea.

ITER is an experimental fusion reactor based on the Tokamak-concept – a toroidal magnetic configuration, where the conditions for controlled fusion reactions are created and maintained. Superconducting magnet coils around a toroidal vessel shall confine and control the plasma and induce an electrical current (15 MA) through it. Fusion reactions take place when the plasma is hot enough (3 .. 4 keV), dense enough ($n = 7 \cdot 10^{20}$ .. $9 \cdot 10^{20}$ m^{-3}), and contained long enough ($\tau \approx 100$ s) for the atomic nuclei (in case of ITER deuterium and tritium) in the plasma to start fusing together. These facts, formulated by J. D. Lawson in 1957, mean: $n\tau \geq 10^{20}$ m^{-3}s.

The aims of this fusion reactor are to produce an inductively driven plasma burn at a fusion power level of 500 MW for 400 s and to extend the burn ultimately to steady state through the use of non-inductive current drive by neutral particle beams and microwaves.

One of the most important performance figures is the ratio Q of the thermal power released from the plasma to the thermal power input into the plasma. This value will be between 5 and 10 in ITER.

1.2 Design of ITER

The main design features of ITER are shown schematically in figure 1. The superconducting toroidal field (TF) magnet consists of eighteen D-shaped coils containing circular cross-section conductors, composed of Nb_3Sn strands, embedded in grooved radial plates. The central solenoid (CS) uses square cross-section Nb_3Sn conductors and has six modules, which can be powered separately. The six poloidal field (PF) coils are made of NbTi-conductors in double pancakes. The lower PF coils are designed with redundant turns and a margin in current to avoid the need to replace the coils in case of local damage in one of the coil pancakes. To accommodate field errors due to manufacturing inaccuracies or to misalignment during the assembly of the magnet coils, as well as to control resistive wall mode plasma instabilities, superconducting saddle-shaped correction coils are placed around the machine outside the TF magnets.

When energised, the TF coils press together along their straight sections,

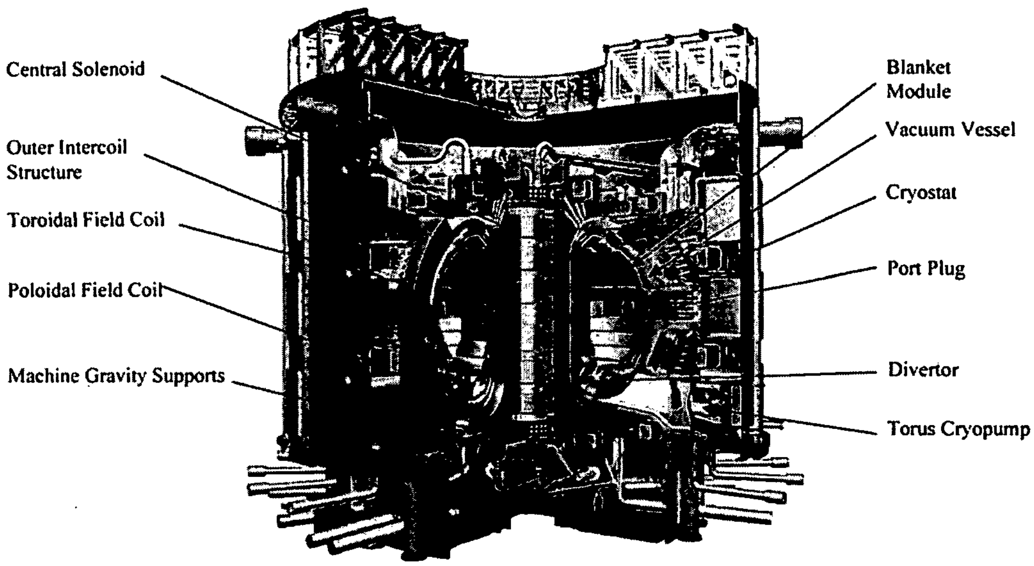

Figure 1: Cutaway of ITER-Tokamak inside the cryostat. (Published with kind permission of ITER.)

forming a vault. The coils are encased to aid their support and to transfer loads across keys between the cases. The poloidal magnetic field crossing the TF coils creates overturning moments and circumferential torques on each TF coil. A shell-like structure between the coils permits these forces to be reacted within the magnet structure and provides a strong support for the PF coils.

The reaction chamber consists of a vacuum vessel supporting remotely exchangeable modular in-vessel components. The vacuum vessel consists of nine toroidal sectors, joined by field welds. The vessel is a double-walled stainless steel welded ribbed shell, with internal shield plates and ferromagnetic inserts to reduce the toroidal field ripple. The 421 blanket modules have a single-curvature faceted separate first wall attached to the vessel through 3 cm diameter access holes in the first wall. To accommodate differential thermal expansion and electromagnetic loads, these attachments are stiff radially, but flexible transversely. The plasma-facing components are beryllium armour attached to a copper substrate, mounted on a water-cooled stainless steel support. The outboard modules may later be replaced by tritium-breeding modules. The 54-cassette single null divertor has carbon targets and tungsten high heat flux components, again mounted on a copper substrate, and a water-cooled stainless steel structure bolted to rails on the vessel floor. The targets can accommodate heat loads of more than 20 MWm^{-2} for twenty seconds, but the more normal peak heat load will be 5 .. 10 MWm^{-2}.

Six of the seventeen accessible vessel equatorial port plugs are used for heating antennae and neutral beam ducts, three are used for power reactor test blankets, two for plasma limiters, and the remainder for plasma diagnostics. The limiter and two diagnostic ports are also used for remote blanket module replacement. Nine divertor ports accommodate eight torus cryopumps, diagnostics, a glow-discharge cleaning system, pellet and gas injection, and an in-vessel viewing system. Three divertor ports are also used for the remote replacement of the divertor cassettes, which are inserted radially and then slid toroidally and clamped to rails. The eighteen upper ports are mainly used for diagnostics. Three of them contain electron cyclotron antennae to control plasma instabilities.

A cryostat surrounds the coils. It is essentially a reinforced single-shell cylinder with 24 m in height and 28 m in diameter. Shielding thicknesses are arranged to permit personnel access to the port terminations or, exceptionally, for repairs in the cryostat-coil interspace after shutdown. To reduce heat inleak to the coils from radiation from surrounding warm surfaces, thermal shields are used between the vacuum vessel and the TF coils.

The Tokamak is water-cooled by separate circuits feeding the blanket (three circuits in parallel), divertor and limiter (one circuit), and vacuum vessel (two circuits in parallel). The vessel circuit itself can remove, by natural convection, all decay heat after shutdown in all vessel and in-vessel components. Typical water inlet temperature is 100 °C, and pressures are in the range of 3 .. 4.2 MPa. Baking of in-vessel components to remove adsorbed impurities is carried out at 240 °C (200 °C for the vessel).

The plasma is heated (and current may be driven) by a combination of electron cyclotron, ion cyclotron, lower hybrid and 1 MeV negative-ion-accelerated neutral beam systems. The initial setup will involve two neutral beams and electron and cyclotron systems, but the radio-frequency systems are designed in exchangeable modular units (20 MW per port) to allow various mixtures to be tried, and three neutral beams can be accommodated on the machine. A heating power in excess of 110 MW is thus attainable.

ITER is assembled inside a cylindrical "pit", embedded up to the equatorial port level. After installation of the lower cryostat, PF coils and supports, 40° sectors of the vacuum vessel are combined with two TF coils and appropriate thermal shielding, and welded to adjacent sectors in the pit. The upper coils, ports and services are connected, and the cryostat is closed by a flat lid with heavy segmented shielding.

1.3 Toroidal field model coil

The objective of the Toroidal Field Model Coil (TFMC) Project (led by the EU) was to develop and demonstrate the superconducting magnet technology to a level that would allow the ITER TF coils to be built with confidence. It allowed design and analysis to be validated, industrial manufacturing methods to be demonstrated, confirmed the performance of each component integrated in the magnet, and tested and demonstrated reliable operation.

The project was aimed at defining the critical steps in this process by the manufacture of a subsize coil, about 4 m high and 3 m wide, and two full-size sections of the outer housing, including the key technical features and manufacturing approaches foreseen for the actual ITER TF coils. Because only a single coil was made, the conductor cannot be fully tested for superconducting properties (this was done instead by testing a TF insert coil in the CS model coil), and the manufacturing was done to define appropriate tolerance targets, procedures and quality control steps. The test of the subsize coil creates realistic magnetic loads to demonstrate the structural concept.

The assembly of the winding pack was completed in 1999. The impregnation of the individual radial plates with an outer insulation wrap was finished in July 2000 and the outer joints between pancakes were electron beam welded in August 2000. When the winding pack was put into the case and closure welded, problems were found initially with the weld quality, but this was resolved by the supplier. Vacuum impregnation of the winding pack-case gap (pre-filled with coated sand granules) was completed in late 2000 and the finished coil delivered to the TOSKA facility at Karlsruhe, Germany, which had been adapted to accommodate the coil and its test programme.

Assembly and checking of the coil in TOSKA (figure 2) was completed in June 2001. The coil for the first time was cooled down to become superconducting in July 2001; it was ramped to 80 kA (above the value needed in ITER and the maximum possible in the facility) with a magnetic field of 8 T. This is the highest current ever driven in a superconducting coil. All joints and the superconductor behaved as expected, as did temperature in-

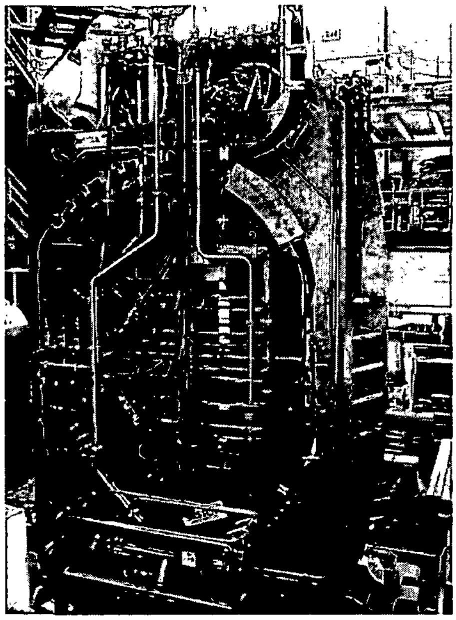

Figure 2: Complete TF model coil prepared for low-temperature tests. (Published with kind permission of ITER.)

creases during fast ramp-down and safety discharge. Temperature margins were found (also in the CS Model Coil) to be somewhat lower than expected due to strand strain sensitivity, and this has led to a tightening of the strand procurement specification (higher current density) and/or the use of a less contractive jacket material [ITE04].

1.4 Conductors for the Central Solenoid and the Toroidal Field Coil

As mentioned in subsection 1.3, the superconductor for both the central solenoid and the toroidal field coils is a Nb_3Sn cable-in-conduit type with a central cooling channel, cooled by supercritical helium. Each single strand has a diameter of 0.81 mm and is Cr-plated to avoid sintering between the strands during the reaction heat treatment, which would lead to unacceptably high coupling losses in the pulsed magnetic fields. Approximately 1000 strands are cabled together with a multi-stage arrangement in five stages to form a cable with a current carrying capability of up to 80 kA. The cable is then enclosed in a jacket made of a nickel-based superalloy, known as Incoloy 908, with a square outer section for the CS model coil (see figure 3) and in a circular stainless steel jacket for the TF model coil, using a pull-through and compaction process. The qualification of the large scale production of

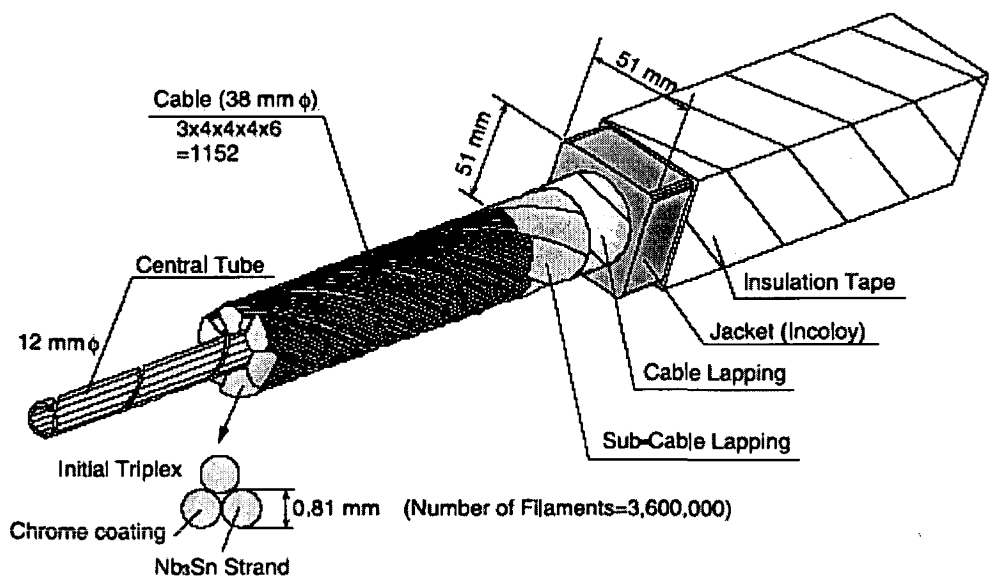

Figure 3: 40 kA – 13 T Nb_3Sn conductor for the CS model coil. (Taken from [Tsu01].)

Nb_3Sn strands to a reproducible performance level, which additionally satisfies the requirements for high current densities and low hysteresis losses, as well as the establishment of the full conductor manufacturing process including cabling and jacketing were done by [Tsu01].

The design requirements for the Nb_3Sn strands were split into two categories: the high performance-I (HP-I) requirement, where a critical current density of $j_c > 700$ kAmm^{-2} in a magnetic field of 12 T and hysteresis losses for a magnetic cycle between 3 T and -3 T of $Q_0 < 600$ kJm^{-3} – non Cu are demanded and the high performance-II (HP-II) requirement with $j_c > 550$ kAmm^{-2} (also with $B = 12$ T) and $Q_0 < 200$ kJm^{-3} – non-Cu.

When the ITER Engineering Design Activities (EDA) were initiated in July 1992, four strand production technologies had been developed:

1. the internal tin method, in which niobium and tin filaments are placed in a copper matrix,

2. the bronze method, in which niobium filaments are placed in a bronze matrix,

3. the tube method, in which small tubes of niobium are filled with a tin core and then placed in a copper matrix, and

4. the jelly roll method, in which grids of niobium are rolled up with sheets of tin.

In all methods Nb_3Sn filaments are formed by a reaction heat treatment at around 650 °C.

From these four technologies two manufacturing processes were adopted: Furukawa (Japan), Hitachi Cable (Japan), Vacuumschmelze (VAC, EU) and VNIINM (Russia) used the bronze process, whereas Mitsubishi (Japan), IGC (USA) and Europa Metalli (EM, EU) used the internal tin process ([Bru96], [Shi98]). The number of Nb_3Sn filaments in the strands is in the range of 4000 – 9000, and their diameters are between 2 μm and 5 μm. As a diffusion barrier Ta or a combination of Ta and Nb are used. Figure 4 shows the cross section of an internal tin single strand produced by Europa Metalli.

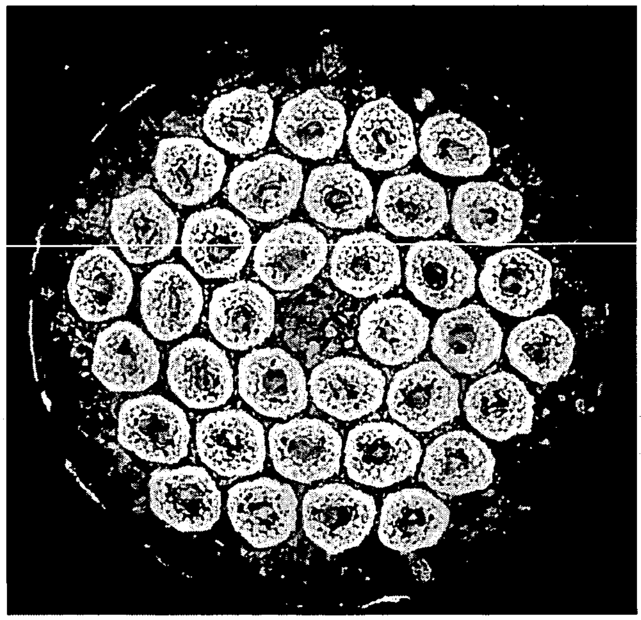

Figure 4: Cross sectional view of a Nb_3Sn single strand produced by Europa Metalli.

The strand development started in 1993. In the first step definitions of the quality assurance were made. Then a trial production of 0.5 t of a strand, followed by the demonstration of 0.5 t manufacture, were carried out. The last of the four development stages was the production of the CS and TF model coils, done in 1997.

A total amount of 24 t of Nb_3Sn strand for the CS model coil and 4 t for the TF model coil were produced. The suppliers were generally able to fulfil the ITER HP-II requirements within a margin. For ITER HP-I, it was sometimes possible to exceed the critical current density specification, but more difficult to meet the requirement for hysteresis losses.

It was not very difficult to achieve a high critical current density around $j_c = 1000$ Amm^{-2} by the tube method; the hysteresis losses in strands produced by this method were around $Q_0 = 1000$ kJm^{-3} – non-Cu, however. In strands fabricated by the bronze method the hysteresis losses were less than $Q_0 = 200$ kJm^{-3} – non-Cu, but the critical current density had to be enhanced. The strand made by the internal tin method had an intermediate performance with a critical current density of $j_c = 600$ Amm^{-2} and hysteresis losses of around $Q_0 = 400$ kJm^{-3} – strand. In all four processes an enhancement of the properties also tended to be associated with frequent strand breakage, which would have given short and unpredictable unit lengths and excessive wastage in the cabling process, and which therefore had to be avoided. Some 5.6 km of Nb_3Sn 40 .. 50 kA conductor for the CS model

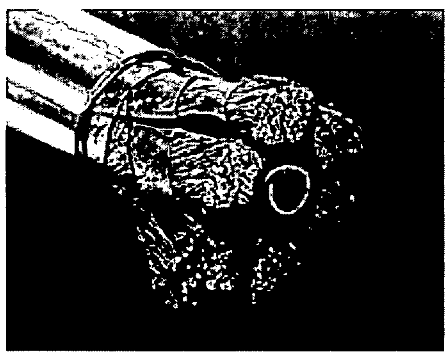

Figure 5: Nb_3Sn cable for the TF model coil. (Taken from [EFD04].)

coil and 1 km of 50 .. 60 kA conductor for the TF model coil (figure 5) have been successfully produced. These conductors were manufactured within a high degree of international collaboration between the partners of the ITER project, involving many industrial companies [Syt99]. During the production, a lot of interface issues, including international transportation and customs clearance problems, as well as quality assurance issues have been successfully overcome, and the experience gained gives confidence that the much larger production required for ITER can be carried out successfully in the future.

1.5 The European Fusion Development Agreement

The European Fusion Development Agreement (EFDA) was established on January 1st, 1999 as a framework contract between EURATOM and its partners in the field of controlled fusion [EFD04]. It is part of a long-term programme of co-operation covering all the activities in the field of fusion research by magnetic confinement in the European Union and in the Swiss Confederation. Recently, some Eastern European countries (i.e. the Czech Republic, Hungary, Latvia and Romania) have also joined the programme.

EFDA is intended to strengthen the co-ordination of work among the associates. It will further develop the necessary scientific, technical and organisational basis in the associations and in the European industry for the possible construction of ITER and will reinforce the European capability for international co-operation.

The EFDA leaders, in the performance of their activities, are assisted by staff members distributed in two so called Close Support Units (CSU), one located at the Max Planck-Institut für Plasmaphysik in Garching, Germany, and the other at the UKAEA laboratory in Culham, UK. These two teams ensure that the collaborative work undertaken by the much larger number of scientists and engineers from the associated laboratories, whether experiments on JET, technology R&D or design tasks for ITER, the international project, is fully integrated into the overall European fusion programme.

The Institute of Solid State Physics at Vienna University of Technology has been part of one of the European Associations, namely the Austrian Academy of Sciences (Österreichische Akademie der Wissenschaften, ÖAW) for several years [OAW02]. To give some examples, the working group for superconductivity has been member of the EFDA Technology Workprogramme 2000 with the task title "Materials for Superconducting Fusion Magnets (SUCOFU)". Another task, that was worked on at Vienna University of Technology, belonged to the EFDA Technology Workprogramme 2001 and had the title "Cable and Conductor Characterisation (EFDA reference: TW1-TMC/SCABLE)". A third example for the cooperation of the Institute of Solid State Physics (until December 31st, 2001 Institute of Experimental Physics) with the EFDA is the Working Programme 2003 with the task entitled "Test of Advanced Nb_3Sn Strands (EFDA reference: TW3-TMSC-ASTEST)". The appropriate contract was signed in December 2003 and will be accomplished by the end of 2004.

At present, the ITER project, which already 200 million Euros are foreseen for in the sixth framework programme, is deadlocked by the still open decision of the site for ITER in France or Japan.

2 Properties and heat treatment of the investigated strands

2.1 Layout information and performance parameters of Nb_3Sn strands

All the work performed in the framework of the technology tasks mentioned in subsection 1.5, was focussed on the investigation of Nb_3Sn strands, produced either by Europa Metalli (henceforth referred to as EM) or by Vacuumschmelze (henceforth referred to as VAC). The former is located in Fornaci di Barga, Italy, the latter in Hanau, Germany. In table 1 some layout information on both strand types are given.

Table 1: Layout information on EM and VAC Nb_3Sn single strands.

Manufacturer	Europa Metalli	Vacuumschmelze
sample identification no.	NET/92-83/B/4A1/ 285-17/M/A	16/72/5740
production technique	internal tin	bronze
no. of filament bundles	36	55
no. of filaments	$36 \cdot 150 = 5400$	$55 \cdot 85 = 4675$
diffusion barrier	multiple Nb-Ta barriers	Ta monobarrier
stabiliser	Cu	Cu
diameter	0.81 mm	0.81 mm
external coating	Cr	Cr

Prior to any measurement, the strands have to be heat treated in order to form the superconductor (Nb_3Sn). The reaction heat treatment parameters are given by the producers: EM strands have to be reacted for 200 h at 210 °C and for 180 h at 650 °C, whereas the heat treatment suggested by VAC is 220 h at 570 °C and 175 h at 650 °C. These are the standard heat treatment cycles, which deliver superconducting strands with the performance parameters given in table 2.

Table 2: Performance parameters of EM and VAC strands.

Manufacturer	Europa Metalli	Vacuumschmelze
j_c (non-Cu)	> 700 Amm^{-2} at B = 12 T, T = 4.2 K	> 600 Amm^{-2} at B = 12 T, T = 4.2 K
Cu : non-Cu ratio	1.5	1.5
Q_0 ($\pm$ 3 T cycle)	< 600 kJm^{-3}	< 200 kJm^{-3}
RRR	> 100	> 100

Q_0 denotes the hysteresis losses, measured in a magnetic field cycle between -3 T and +3 T. The residual resistance ratio or – abbreviated – *RRR* is defined as the ratio of the electrical resistivity at room temperature and the electrical resistivity just above the critical temperature T_c.

From the diameter of a strand (d = 0.81 mm for both EM and VAC strands) and the copper to non-copper ratio of 1.5 the cross sectional area of a strand can be calculated to be $A = \frac{\pi d^2}{4} \approx 0.5153$ mm^2. This gives the fraction of the non-copper cross sectional area of $A_{\text{non-Cu}} \approx 0.2061$ mm^2 and the fraction of the copper cross sectional area of $A_{\text{Cu}} \approx 0.3092$ mm^2. The distinction between non-copper and copper cross sectional area is important for the determination of the critical current density j_c after measurement of the critical current I_c. It is a matter of fact that one can only measure critical *currents* in an experiment; the appropriate critical current *densities* have to be determined afterwards. In table 2 the critical current density j_c is given with respect to the non-copper cross sectional area of a strand. This accounts for the fact that in the superconducting state no current is going through the copper cross sectional area of the strand, as the strand acts as a parallel connection of two resistors – one of them the copper with finite resistivity, the other the superconductor with zero resistivity. This results in a zero total resistivity. Therefore the correct current density is obtained by dividing the measured value of I_c by the non-copper cross sectional area $A_{\text{non-Cu}}$:

$$j_c = \frac{I_c}{A_{\text{non-Cu}}}. \tag{1}$$

2.2 Heat treatment of Nb_3Sn strands

The reaction heat treatment of EM and VAC samples has been performed in the Institute of Solid State Physics (formerly Institute of Experimental Physics) at Vienna University of Technology. For this purpose the following equipment is available, shown in figure 6:

- two furnaces (MEDLIN-Naber L47T and MEDLIN-Naber N11 with $P_{\text{max}} = 3.3$ kW and $T_{\text{max}} = 1100$ °C),
- two digital PID temperature controllers (Eurotherm 2408 with 16 programmable ramp sections),
- one digital temperature recorder (Eurotherm CHESSELL 4100G with 6 analogue input channels),
- up to four reaction tubes made of high-grade steel, equipped with radiation shields, for insertion into the furnaces,

- two S-type thermocouples (Pt-Rh) on the rear walls of the furnaces, and
- four E-type thermocouples (NiCr-CuNi) inside the reaction tubes.

The annealing processes are carried out in argon-atmosphere, starting with a pressure of $\approx$ 400 mbar at room temperature. In each heat treatment cycle

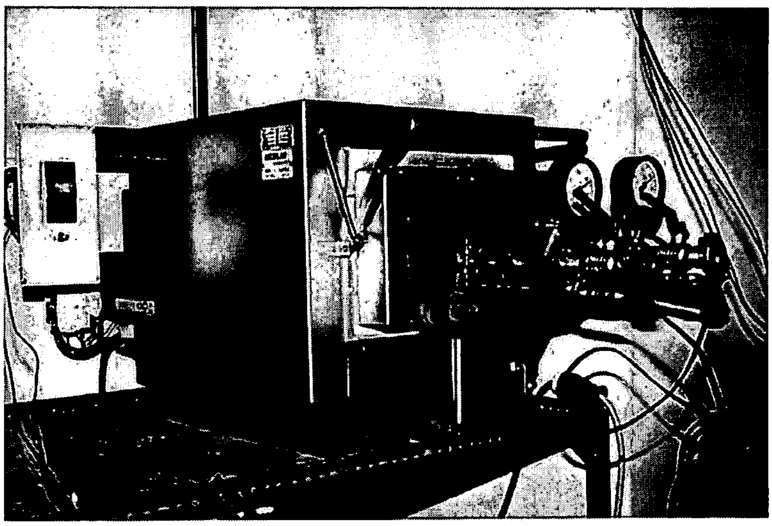

Figure 6: Heat treatment equipment in the Institute of Solid State Physics.

up to four samples for I_c measurements and up to two samples for hysteresis loss measurements can be reacted simultaneously with an individual heat treatment programme in each furnace. The two furnaces mentioned above are used for full heat treatment cycles. Optionally, a third one can be used for cooling down samples, which are removed from one of the reaction furnaces in order to have a last reaction step being shorter than the last step programmed on the PID temperature controller. The temperature stability and homogeneity in the PID-controlled furnaces from Eurotherm is better than ±1 °C during the ramp periods and better than ±0.5 °C during the dwell periods. The ramp rate is always chosen to be 10 Kh^{-1} in order to fulfil the ITER requirements.

2.3 Optimisation of the reaction heat treatment of EM and VAC Nb_3Sn strands

The heat treatment cycles of Nb_3Sn strands, predetermined by the manufacturers, are mainly designed to achieve the highest possible critical currents and therefore very long: as mentioned in section 2.1, the heat treatment recommended by EM is 200 h at 210 °C and 180 h at 650 °C. A similarly long two-step cycle is recommended by VAC: 220 h at 570 °C and 175 h at 650 °C. Due to the manufacturing requirements of cleanliness two additional steps – 24 h at 340 °C and 24 h at 450 °C – are necessary for both strand types. This adds up to a total heat treatment time of 554 h (i. e. 23 days and 2 hours) for EM strands and 569 h (i. e. 23 days and 17 hours) for VAC strands, including the ramping times at a ramping rate of 10 Kh^{-1}. These long time spans result in a considerable delay in the manufacturing process of very large superconducting magnet coil systems as they are necessary for the toroidal field (TF) coils and the central solenoid (CS) in ITER.

Hence, it is of interest to investigate whether a shorter heat treatment cycle delivers superconducting strands with the same or at least nearly the same performance as it is obtained by long heat treatment cycles. For this reason Nb_3Sn strands made by EM and VAC had to undergo various heat treatments (see table 3) and subsequently characterised with respect to their critical currents, hysteresis losses, and residual resistance ratio ([Foi01], [Hen03]). The optimisation of the heat treatment has been carried out within Association EURATOM-ÖAW (Austrian Academy of Sciences), Technology Task TW1-TMC/SCABLE (see section 1.5). The results of those studies are shown in figures 7 and 8.

Table 3: Dwell time and final annealing temperature of the heat treatments performed (s. c. denotes the standard cycle recommended by VAC).

dwell time (hours)	annealing temperature (°C)				
	640	650	660	675	690
25				√	
50		√		√	
75				√	
100		√		√	
120	√	√	√	√	
150		√		√	
175		s. c.			
200	√	√	√	√	√
240	√	√	√	√	

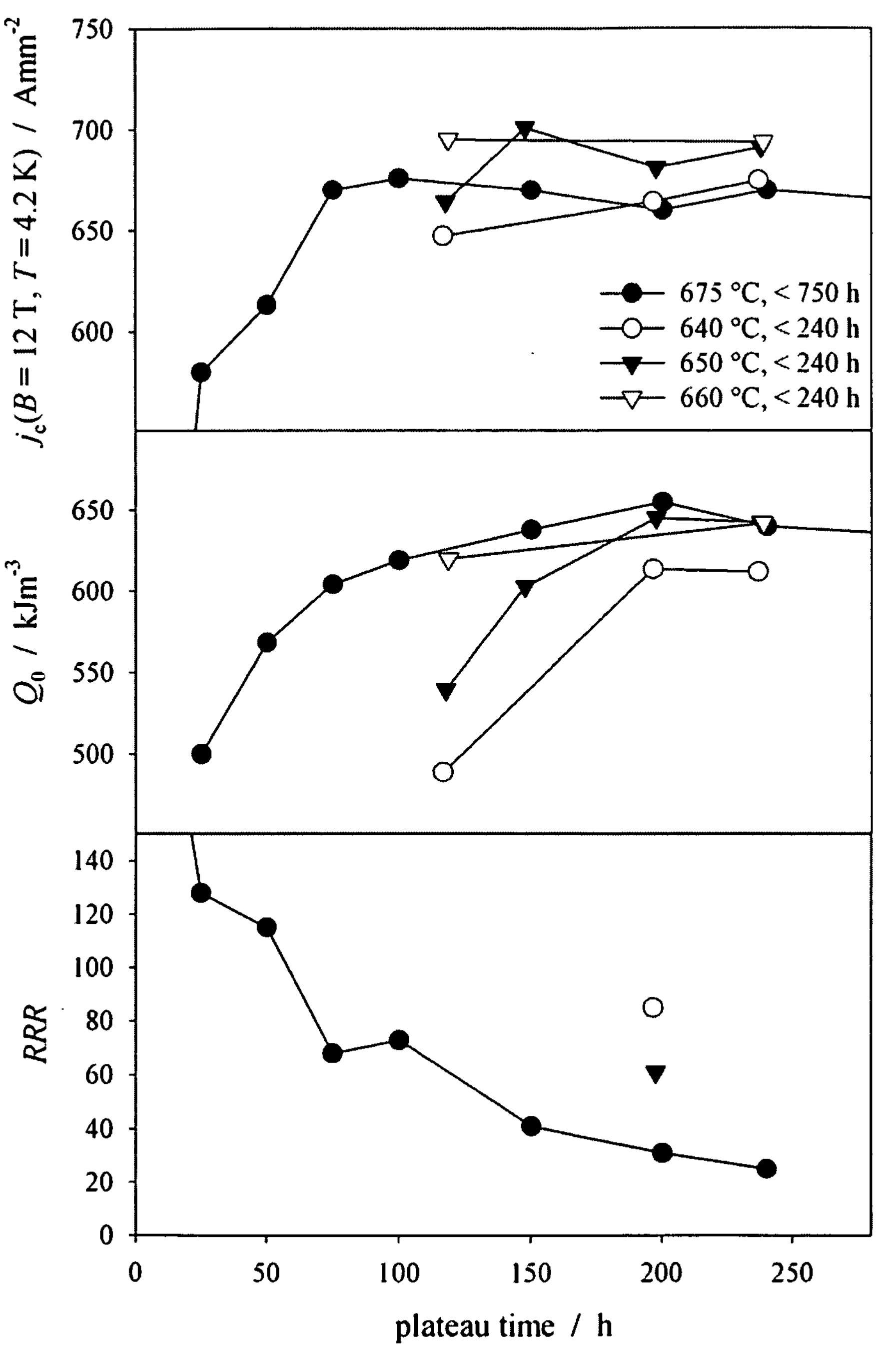

Figure 7: Critical current density, hysteresis losses, and residual resistance ratio of EM strands as a function of the plateau time.

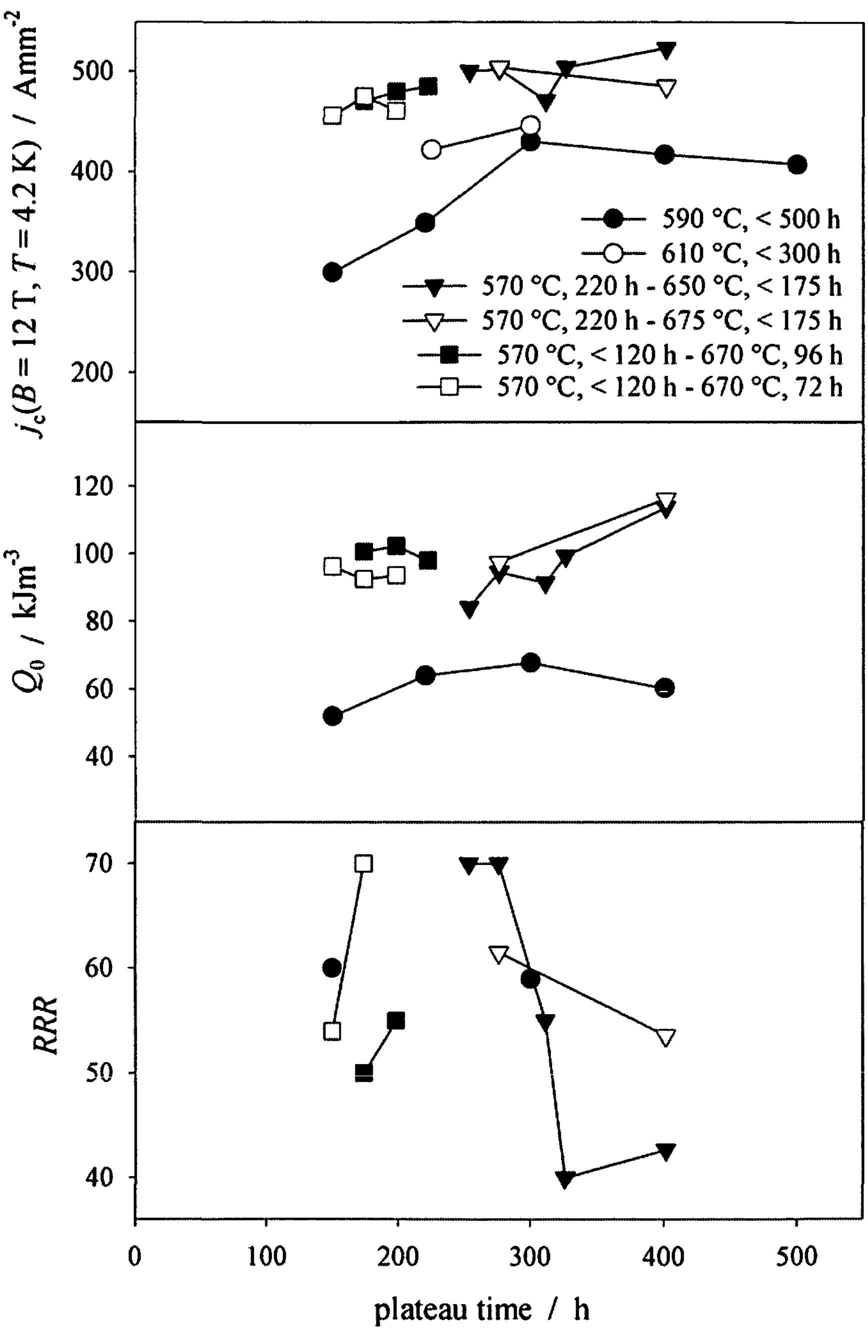

Figure 8: Critical current density, hysteresis losses, and residual resistance ratio of VAC strands as a function of the plateau time.

Discussion of the results

(1) Critical current density j_c:

(1a) *Results for EM internal tin strands*

After a certain annealing time a plateau of j_c is reached, showing only a little change in j_c with increasing annealing time. The higher the temperature, the earlier the plateau is reached. On the j_c-plateau, deviations from the annealing temperature of the order of ±10 °C hardly effect j_c.

(1b) *Results for VAC bronze route strands*

Due to the limited tin content in the bronze, the critical current densities are distinctly lower in comparison to those obtained for the internal tin strands. The heat treatment cycle recommended for VAC strands is planned to consist of two steps: one at 570 °C, followed by one at 650 °C. Also in this case a j_c-plateau is reached soon after the beginning of the annealing step at 650 °C, with a slight increase of j_c with the annealing time. At 675 °C the behaviour is almost the same.

The attempt of reaching the same level of critical current density with only one annealing step at 590 °C failed. With increasing annealing time j_c becomes larger, until a maximum in j_c is reached. Nevertheless, with short heat treatment steps (both steps being approximately half as long as recommended by VAC) a plateau is reached on nearly the same level as in case of long annealing steps.

(2) Hysteresis losses Q_0:

In figures 7 and 8 the hysteresis losses are shown related to the non-copper volume of the superconductors as a function of the annealing temperature. It is evident that Q_0 grows with increasing annealing temperature and duration. The losses are distinctly higher in case of EM strands, exceeding the ITER HP-I specification of $Q_0 < 600$ kJm^{-3} by 5 .. 10 % if the strands are reacted for 200 h at 650 °C. After annealing for 120 h at 650 °C, the j_c-plateau is already reached, but the hysteresis losses are below the limit.

For VAC strands, the losses are much smaller and easily fit into the ITER HP-II limit of $Q_0 < 200$ kJm^{-3}.

(3) Residual resistance ratio (RRR):

It can clearly be seen that the residual resistance ratios are dropping with increasing annealing temperature and duration for both strand types. EM as well as VAC strands do not comply with the ITER requirement of $RRR > 100$.

It has been demonstrated that nearly the same critical current densities in Nb_3Sn strands by EM and VAC can be achieved with a heat treatment cycle being 100 .. 200 h shorter than recommended by the strand producers. At the same time there is a benefit of lower hysteresis losses for EM strands, which is considerable and brings them into the margins of the ITER HP-I specification. Furthermore, the residual resistance ratio becomes distinctly smaller after shorter annealing procedures.

Concluding, it can be estimated that the overall time for the heat treatment of all ITER TF coil segments will be shortened by nearly one year, using the optimised strand reaction cycles. Beside this benefit to the schedule there will be a noticeable reduction of production costs and lesser risk of heat treatment failures. Therefore it is proposed that each strand supplier defines the parameters for an individual heat treatment cycle, that has been optimised with respect to j_c, Q_0, and RRR of not more than 400 h duration, including ramping times.

2.4 Unified heat treatment of EM and VAC strands

Under consideration of the data obtained for EM and VAC strands, it was possible to design a standardised heat treatment cycle which allows strands of both manufacturers to be annealed together and at the same time, leading to satisfactory results in critical current density, hysteresis losses, and residual resistance ratio. The optimised and unified heat treatment is given in table 4. A comparison of the heat treatment cycles recommended by EM and VAC respectively to the unified heat treatment process is shown graphically in figure 9.

Table 4: Unified reaction heat treatment cycle for EM and VAC strands.

temperature / °C	210	340	450	570	670
dwell time / h	100	24	24	96	96

Additionally, the samples have been subjected to heat treatments at 670 °C for 0 h, 24 h, 48 h, 72 h, 120 h, and 150 h. A shorter annealing time than 72 h does not seem to be reasonable due to incomplete reaction of the filaments in this case as well as a reduction of the critical temperature. Incomplete reaction of a strand is shown in figure 10, where the unreacted

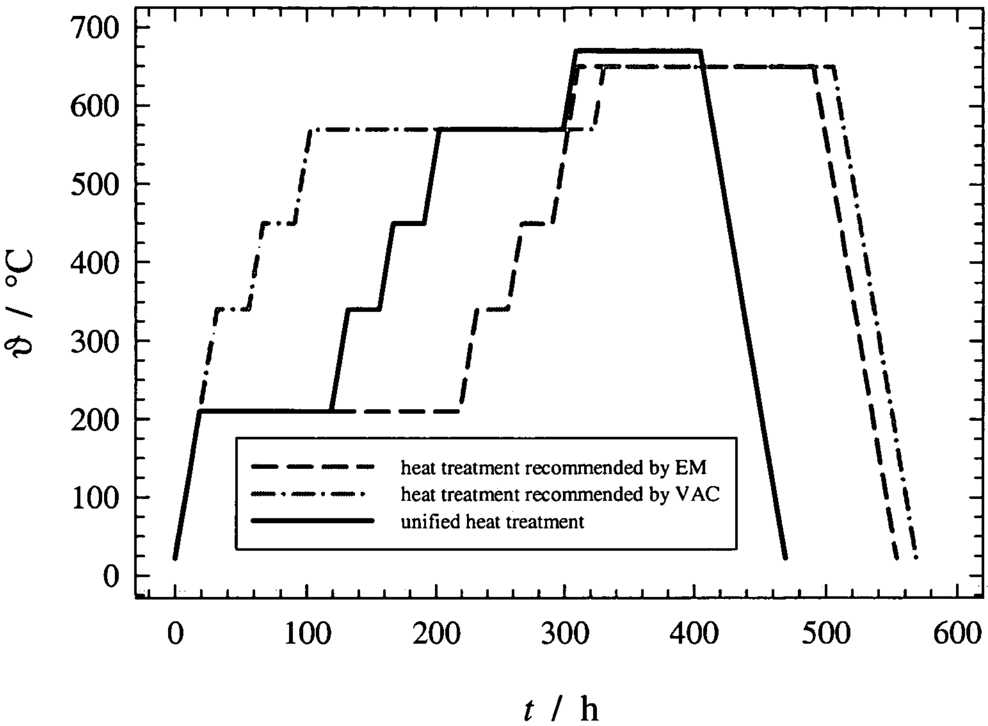

Figure 9: Comparison of the heat treatment cycles recommended by EM and VAC to the unified cycle.

tin cores of the filaments can easily be seen. The sample is an internal tin strand from EM, which has not been heat treated at 670 °C. Figure 11 shows completely reacted filaments in an EM strand, reacted after the unified heat treatment cycle mentioned above (96 h at 670 °C). Figures 10 and 11 are SEM micrographs, taken from a JEOL JSM-5410 scanning electron microscope.

Using this unified reaction heat treatment cycle, the total annealing time is reduced to 470 h (i.e. 19 days and 14 hours, including ramping times) in comparison to the heat treatment cycles recommended by the manufacturers

Europa Metalli and Vacuumschmelze (554 h and 569 h, respectively), leading to a time saving in each reaction procedure of almost one week.

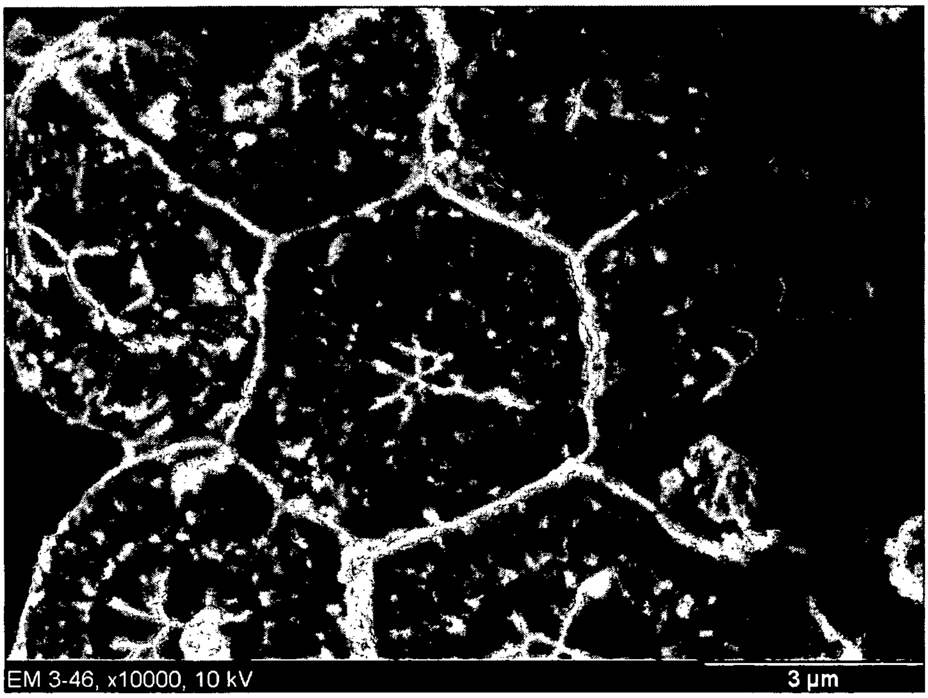

Figure 10: Unreacted tin cores in the filaments of an EM strand, 10000-times magnified.

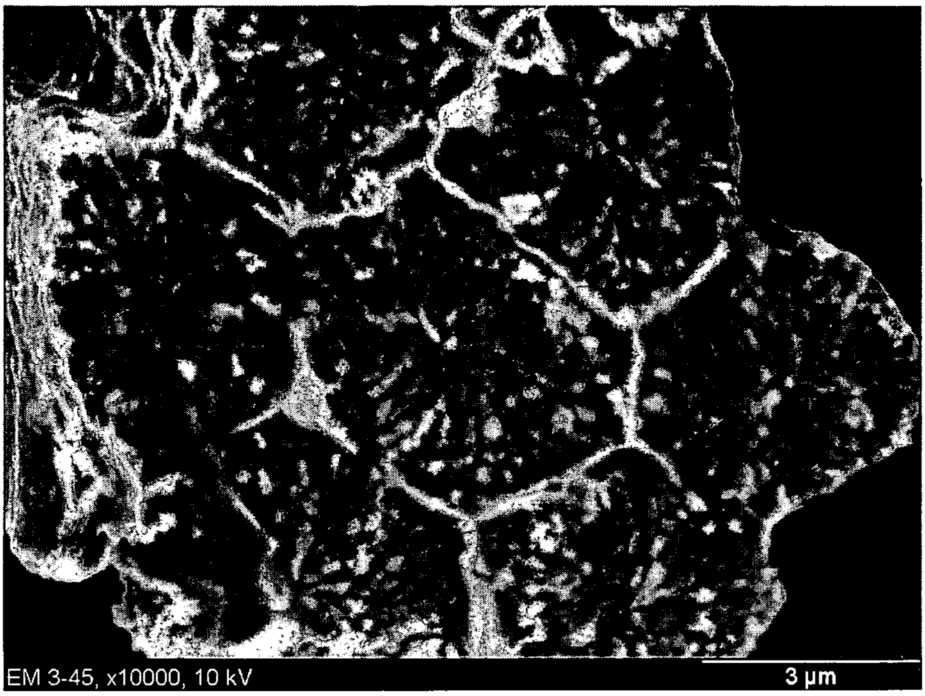

Figure 11: Completely reacted filaments in an EM strand, heat treated by the unified reaction cycle, 10000-times magnified.

3 Sample preparation and measurement of U-I-, U-B-, and U-T-characteristics

3.1 Sample holder for I_c-, B_c-, and T_c-measurements

The standard sample holder for critical current measurements was developed by the "NET/ITER-team for the characterisation of superconducting strands for fusion applications" during the second ITER strand benchmark test. It consists of a threaded hollow cylinder between two copper rings. A sketch of the holder is shown in figure 12. The material of the sample holder has been

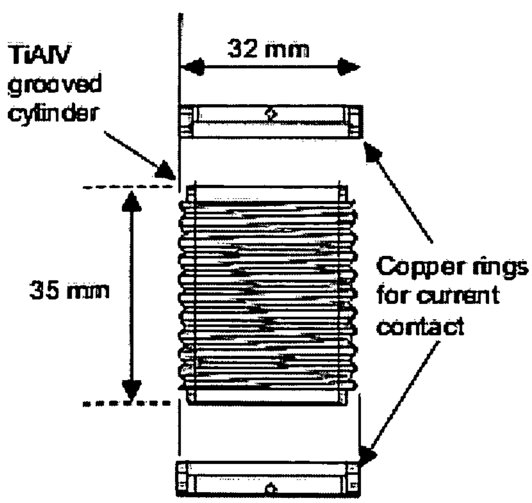

Figure 12: Ti_6Al_4V hollow cylinder with copper rings.

chosen to be Ti_6Al_4V because of the thermal expansion coefficient, matching that of Nb_3Sn, and because of the high resistivity of $\rho \approx 1.4 \cdot 10^{-6}$ Ωm. The reference dimensions of the hollow cylinder are:

- overall height: $h = 35$ mm,
- outer diameter: $d_{\text{out}} = 32$ mm, and
- inner diameter: $d_{\text{in}} = 28$ mm.

The thread is V-shaped with an angle of 90° and a depth of 1 mm. It has eight turns per inch. A section of a Nb_3Sn strand is wound on the sample holder. Using this type of sample holder, called ITER standard barrel, the sample can be heat treated and measured without being transferred from one holder to another. Thus, damaging of the sample due to the brittleness of Nb_3Sn is prevented.

In order to reach those demands, a new type of sample holder was developed in the Institute of Solid State Physics (see figure 13). It has the same dimensions and properties as the sample holder suggested by the NET/ITER-team, with seven turns per inch. The current leads are also made from copper and directly welded on the two copper rings, which are screwed on the Ti_6Al_4V hollow cylinder, each with two M2.5×10 screws.

A 1.2 m long section of Nb_3Sn strand can be wound on this sample holder. The ends of the strand are fixed to the copper rings with two M2.5×10 screws. For measurement, three voltage taps are soldered on the strand: the first 35 cm from the end of the strand, the second 25 cm from the first tap, and the third another 25 cm from the second one.

3.2 Preparation of the samples for heat treatment

As mentioned in subsection 3.1, each Nb_3Sn single strand is heat treated and measured on the same sample holder. For this reason it has to be assembled

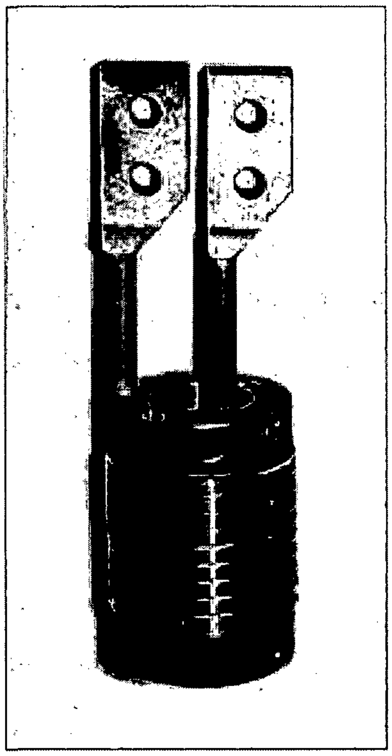

Figure 13: Modified ITER standard barrel: Ti_6Al_4V hollow cylinder between two copper rings; the current leads are welded on the rings.

to the holder before the annealing procedure. The chromium coating has to be removed from the surface of the strand by etching with hydrochloric acid (HCl) in the following places: at the endings, which are soldered to the copper rings after the heat treatment, and at those points, where the voltage taps are attached. After etching, the strand is rinsed with water, dried, and wound under tension on the sample holder. It must be unable to move in the groove. Then the heat treatment is carried out.

End effects, such as tin outflow from the ends, affecting the strand performance negatively are assumed to be limited to the last 10 .. 20 mm of the strand, which are cut away after the heat treatment. After the reaction, one of the strand ends is released, and the strand is checked for bonded contact points on the sample holder. If necessary, it is tightened into the groove, and the end is fixed again.

Finally, the strand ends are soldered to the copper rings in a way that the soldered length is about three quarters of a turn ($\approx$ 75 mm), but not shorter than 60 mm.

3.3 The measuring system

All measurements of Nb_3Sn strands for ITER carried out in the Institute of Solid State Physics within the scope of this doctoral thesis have been performed in a measuring system consisting of the following components:

- OXFORD Cryostat with a Nb_3Sn magnet ($B_{\max}(T = 4.2\text{ K}) = 14$ T, or using the lambda plate refrigerator, $B_{\max}(T = 2.2\text{ K}) = 16$ T) and variable temperature insert (VTI) for a temperature range from 1.6 K up to 300 K. The bore diameter of the VTI is 6.35 cm (2.5 inches),
- OXFORD ITC 503 Intelligent Temperature Controller with three measuring channels and a gas flow control for the VTI,
- OXFORD Lambda Controller for cooling down the helium bath to 2.2 K in order to generate a magnetic field greater than 14 T,
- OXFORD IPS 120-10 Intelligent Power Supply for the magnet,
- OXFORD ILM Intelligent Level Meter to watch the helium level in the cryostat,
- two SIEMENS NTN 35000-20 remotely controllable current generators (each with $I_{\max} = 1500$ A),

- KEITHLEY 182 Sensitive Digital Voltmeter,
- two KEITHLEY 2182 Nanovoltmeters,
- KEITHLEY 196 System DMM voltmeter, and
- personal computer with the operating system Microsoft Windows 2000 and National Instruments LabVIEW 6i for computer-aided measuring process control and automatic measurement data acquisition.

The SIEMENS power sources generate the transport current, flowing through the Nb_3Sn strands. The voltage drop on the sample is measured by the KEITHLEY voltmeters 182 and 2182. The former has one measuring channel and measures the voltage drop between the first and the third voltage tap on the sample, which are 50 cm apart (see subsection 3.1). The latter has two measuring channels, monitoring the voltage drops between the first and the second as well as between the second and the third voltage tap having a distance of 25 cm from each other.

The modified ITER barrel described in subsection 3.1 is mounted on a sample rod that has been developed in the Institute of Electrical Engineering of the Slovak Academy of Sciences. It is capable of carrying a transport current of up to 500 A.

Three temperatures are measured by the ITC 503 temperature controller at three different points: one on the bottom of the VTI, the second one at the head of the sample rod in the VTI, and the third one closely next to the strand. All temperature sensors are CERNOX 61 Ω resistive thermometers, which are compensated for the external magnetic field. The latter is used by channel one of the ITC for controlling and stabilising the sample temperature.

The others deliver insight into the temperature gradient between bottom and top of the VTI. This is important to prevent the current leads on the sample rod from overheating in those cases, when high transport currents are to be expected. The temperature at the head of the sample rod should not exceed ≈ 70 K under usual measurement conditions. The transport currents are measured indirectly by measuring the voltage drop on a shunt. For this reason the KEITHLEY 196 voltmeter is used. The absolute accuracy of the calibrated thermometers is of the order of 100 mK; the relative accuracy is about 1 mK for temperatures below 20 K.

The National Instruments LabVIEW 6i software is capable of controlling and reading all values and parameters from all devices mentioned above. Furthermore, it continuously monitors the voltage drop on the sample (measured by KEITHLEY 182) and stops the measurement (i.e. immediately switches off the transport current) in case a maximum voltage predefined by the experimenter is detected in order to avoid destruction of the sample due to a sample quench.

3.4 Performance of I_c-, B_c-, and T_c-measurements

3.4.1 Measurement of voltage-current-characteristics

The sample temperature is stabilised by the OXFORD ITC 503 PID-controller and kept constant within an interval of 1 % of the measured temperature. The following PID-constants are used for a temperature range up to 30 K: proportional: 30, integral: 0.3, differential: 0. Then, the external magnetic field is set by the OXFORD IPS 120-10, using a ramping rate of 1 T per minute. It is also kept constant. After a waiting time of a few minutes in order to achieve stable temperature condidtions, the transport current is ramped up with a ramping rate of 1 As^{-1}. At the same time the voltage drops are measured between the three voltage taps described in subsection 3.3 twice a second. The current is ramped up, until a voltage drop of 30 μV between the first and the third voltage tap is reached. Then the current is ramped down to zero with the same ramping rate. This procedure ensures that the temperature does not vary too much during the measurement period. If the temperature were not stable, hysteresis could be observed after comparison of the voltage-current characteristics taken with increasing current to the U-I-characteristics taken with decreasing current. In the case of a sample quench the transport current is switched off immediately. A waiting time of five minutes allows to reset and stabilise the sample temperature.

3.4.2 Measurement of voltage-magnetic field-characteristics

For the measurement of voltage-magnetic field-characteristics again the transport current is ramped up to the value desired with a ramping rate of 1 As^{-1}. The sample temperature is set and stabilised in the same way as it is done for U-I-measurements. Transport current as well as the sample temperature are kept constant. The external magnetic field is ramped up to the initial field strength with a ramping rate of 1 T per minute. After the measurement of the voltage drops the magnetic field is increased by 0.02 T, now with a ramping rate of only 0.5 T per minute. This is done in order to keep the electromagnetic induction in the sample as small as possible: every change of the magnetic induction B due to ramping the external magnetic field induces a voltage in the coil-shaped sample, which is given by

$$U_{\text{ind}} = -N\frac{\mathrm{d}\Phi}{\mathrm{d}t} = -NA\frac{\mathrm{d}B}{\mathrm{d}t} \approx -NA\frac{\Delta B}{\Delta t}, \tag{2}$$

where $N = 10$ is the number of windings of the sample on the sample holder, $A \approx 8$ cm^2 is the cross sectional area of the sample, and $\frac{\Delta B}{\Delta t}$ is the change of the magnetic induction with time, determined by the ramping rate. In the case the superconducting sample is close to the transition to normal conductivity, the voltage thus induced can cause the total voltage drop on the sample to exceed the limit of 30 μV, which is used as a criterion for the end of a measurement, even though the effective voltage drop due to temperature, transport current, and stationary external magnetic field is still below 30 μV. In other words: if the magnetic field is ramped up too quickly, the measurement is aborted too early, and only an insufficiently short section of the voltage-magnetic field-characteristic is recorded.

In the course of the experiments it turned out that at a ramping rate of 0.5 T per minute the induced voltage can be estimated to be $U_{\text{ind}} \approx 5$ μV. This is low enough to obtain reasonable U-B-curves, which can be analysed very well.

3.4.3 Measurement of voltage-temperature-characteristics

In the case of measuring voltage-temperature-characteristics, the transport current is ramped up to the desired value with a ramping rate of 1 As^{-1}. The external magnetic field is set in the same way as described in the previous subsection. Both current and magnetic field are kept constant. The initial temperature is set by the PID controller and stabilised for at least ten seconds

within an interval of ± 5 mK before measuring the voltage drops. Then, the temperature is increased by 0.02 K. Again the voltage drops are measured after a stabilisation time of ten seconds. This procedure is repeated, until a voltage drop of 30 μV occurs between the outer voltage taps. If the sample quenches, the transport current is switched off instantaneously.
In the previous three subsections it was described in detail how I_c, B_c-, and T_c-measurements are performed. Some further concluding remarks have to be made, though. The least time-consuming measurements are I_c-measurements. This is due to the fact that in this case first the temperature and the magnetic field are set, which takes some time, and finally the current is ramped up and down. As long as the sample does not quench, once the temperature is set, there is no need for any additional waiting time for stable temperature conditions. Changing the external magnetic field in one-Tesla-steps, starting from 14 T and ending at 8 T, takes one minute per step. The measurement itself, where the voltage drops are recorded while the current is ramped up, takes only a couple of minutes, depending on the sample's critical current at the actual temperature and in the actual magnetic field. For this reason U-I-characteristics are always measured at first to get an overview over the critical parameters of the sample investigated. From the large number of measurements that have been done during the last years and in order to reach the requirements given by EFDA it has been decided that I_c-measurements should be performed in a temperature range from 4.2 K to 9 K and in a magnetic field range from 8 T to 14 T. Since the superconducting coils of ITER are cooled with helium, it is not necessary to study the behaviour of the Nb_3Sn strands below 4.2 K. At 9 K and in a magnetic field of 14 T the critical current of a strand is close to zero. Therefore it is

not necessary to go beyond these limits in temperature and magnetic field. These considerations have led to the following measurement sequence: starting at 9.0 K, seven I_c-measurements are carried out in different magnetic fields (14 T, 13 T, 12 T, 11 T, 10 T, 9 T, and 8 T). Subsequently, the magnetic field is ramped up to 14 T again, and U-I-curves are recorded at 8.2 K. The same is done at 7.4 K, 5.7 K, and 4.2 K. Thus a grid of $5 \cdot 7 = 35$ I_c-values is gained, leading to an insight into the shape of the critical surface of the superconductor.

Starting from here, the measurement parameters for U-B- and U-T-measurements can be determined more easily. The following example may serve to improve the understanding: assume $I_c(B = 12\text{ T}, T = 5.7\text{ K}) = 100$ A. For a voltage-temperature-measurement the magnetic field would be set to 12 T and the transport current would be ramped up to 100 A. The initial temperature does not need to be 4.2 K but can be slightly below 5.7 K, maybe 5.2 K. For a voltage-magnetic field-measurement the temperature would be set to 5.7 K, and the transport current would be ramped up to 100 A. The initial magnetic field does not have to be far away from 12 T, but can be around 11.5 T. In both cases a lot of time saving is achieved, as only close to the transition the characteristics are of particular interest.

The direction of the transport current flowing through the strand is selected in such a manner that the Lorentz force

$$\vec{f} = \vec{j} \times \vec{B} \tag{3}$$

presses the strand towards the sample holder. In equation 3 $\vec{f}$ stands for the force density, i.e. a force per unit volume of the strand, $\vec{j}$ is the current density, and the external magnetic field is denoted by $\vec{B}$.

The voltage criterion for the evaluation of the measured characteristics with respect to their critical magnitudes (I_c, B_c, and T_c) has been chosen to be $U_\mathrm{c} = 0.1\ \mu\mathrm{Vcm}^{-1}$. This means: a straight line is added to the data graph of a measured characteristic parallel to the x-axis (which is the current-, magnetic field- or temperature-axis) at $U = U_\mathrm{c}$, and the intercept point of this line with the measured curve is determined. The x-coordinate of this point is the critical parameter.

As mentioned above, all measurement data are acquired by the LabVIEW 6i software and saved in ASCII format. Datafiles of U-I-measurements consist of four columns, separated by tabulators: the first containing the current through the sample, the others the voltage drops sensed between the three voltage taps on the sample. Information on the external magnetic field and the temperature during the measurement period are contained in the filename.

The data format of files gained after U-B- or U-T-measurements is identical: the first column contains the temperature, the second the external magnetic field, the third the transport current, and into the remaining columns the three voltage drops are written. In this case the columns are separated by tabulators, too.

4 Experimental results of U-I-, U-B-, and U-T-measurements

4.1 General remarks

During the last decades voltage-current characteristics of superconducting Nb_3Sn strands and cables have been examined by many groups. It was found that typical U-I-curves, which are obtained from measurements in the region of the transition from superconductivity to normal conductivity, can be fitted using the following simple power-law:

$$U(I) = k_{(\mathrm{I})} I^n. \tag{4}$$

Here, $k_{(\mathrm{I})}$ and n (called "exponent" or "n-value") are two parameters, which are varied during the least-squares fitting method. In order to simplify the fitting procedure, equation 4 is frequently used in its logarithmic representation:

$$\ln U(I) = \ln k_{(\mathrm{I})} + n \cdot \ln I, \tag{5}$$

since the issue is now reduced to a linear fitting problem. From the fitted curve, it is easily possible to determine the critical current I_c, if some voltage criterion U_c (here: $U_c = 0.1\ \mu\mathrm{Vcm}^{-1}$) is applied:

$$U_c = U(I_c) = k_{(\mathrm{I})} I_c^n \quad \Leftrightarrow \quad I_c = \sqrt[n]{\frac{U_c}{k_{(\mathrm{I})}}}. \tag{6}$$

Some of the groups mentioned in the beginning of this section have reported on characteristic variations of the n-value as a function of temperature and magnetic field ([Ces96], [Kov95]). Furthermore, it has been reported by Warnes et al. ([War86]) that in composite superconductors the transition from the flux-pinning-state to the full flux-flow-state does not happen at one distinct current, but occurs over a range of current. Therefore, the critical current does not have a single, unique value; actually, there is a distribution of critical currents throughout the composite. The critical current range, where the transition from superconductivity to normal conductivity occurs, depends on temperature and magnetic field, too. The narrower it is, the higher is I_c. For this reason, higher n-values are expected in the case of high critical currents.

4.2 Scaling law of the n-value in Nb_3Sn superconductors

In the scope of an optimisation programme of the heat treatment of internal tin and bronze route Nb_3Sn strands used for ITER model coils (see section 2.3), numerous U-I-characteristics for various temperatures, magnetic fields, and heat treatment cycles has been recorded. After a systematic evaluation of these data, it was found quasi as a side effect of I_c-measurements that the n-values of both Europa Metalli and Vacuumschmelze strands behave like a function of the critical current j_c ([Hen03]):

$$n(I_c) = b \cdot I_c^d. \tag{7}$$

Since the the critical current density and, thus, the n-value of a high quality superconductor, one of which is Nb_3Sn, is largely determined by the intrinsic fluxoid-microstructure interactions ([Fäh77]) of the superconducting material, it is possible to investigate the behaviour of those intrinsic interactions by monitoring the correlation of n-values and critical currents. Figure 14 shows a plot of the n-values of EM samples annealed at 675 °C for different heat treatment durations ranging from 1 h to 200 h as a function of the non-copper critical current.

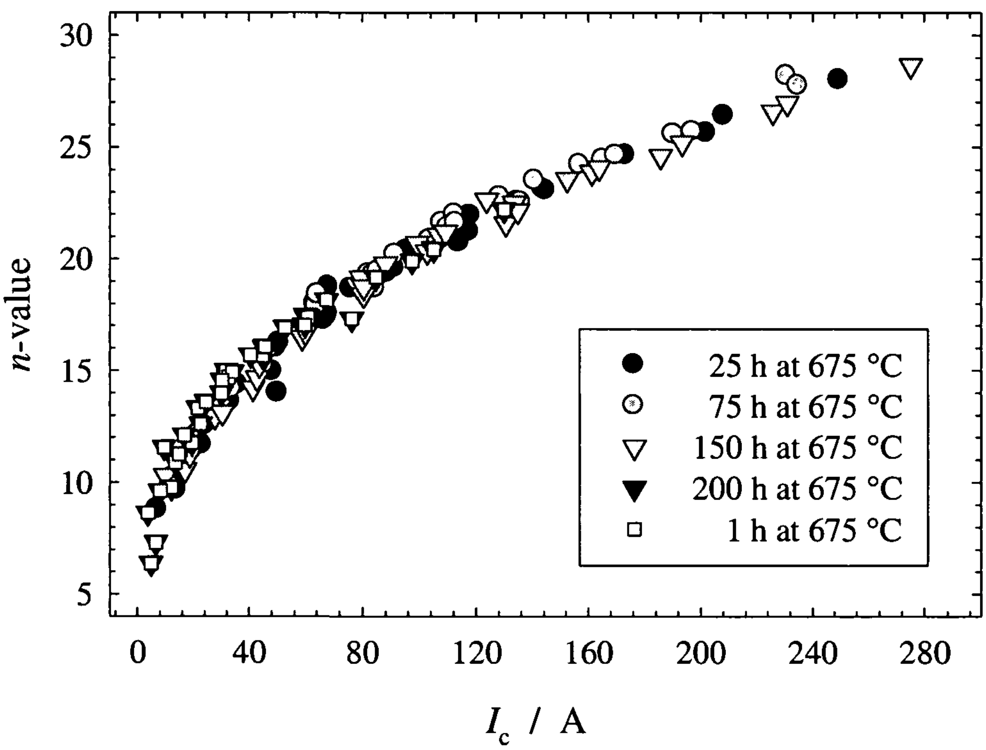

Figure 14: n-value of EM strands annealed at 675 °C as a function of the critical current.

I_c-measurements were performed in a temperature range between 4.2 K and 9 K and in magnetic fields ranging from 8 T to 14 T. A least-squares fit of the n-value-data points obtained from those measurements delivers the parameters b and d used in equation 7. The numerical values are $b = 4.11$ and $d = 0.35$.

From the universal scaling law of the n-value as a function of the critical current density, independently of the heat treatment, the conclusion can be drawn that in internal tin superconductors from EM neither the homogeneity of the superconductor, nor the behaviour of the pinning centers is influenced by the variation of the annealing conditions ([Fil02b]).

Another interesting question is, how the scaling of the n-value behaves for a Nb_3Sn strand with different strand layout. Within the optimisation programme mentioned above, a lot of $I_c(B, T)$-measurements have been performed on VAC bronze route strands, too, and again a scaling law for the exponents n as a function of the non-copper critical current density could be found ([Hen03]). The fit parameters for the scaling of the n-values of VAC strands are $b = 4.73$ and $d = 0.44$. A comparison of the behaviour of the n-values as a function of the critical current density between EM and VAC strands is shown in figure 15. The different symbols are representing different annealing times during the last heat treatment step at 675 °C. In both cases the n-value is only a function of j_c, even though the samples were heat treated under significantly different conditions. Moreover, it can be seen in figure 15 that the n-values of VAC strands are distinctly higher than those obtained for EM strands.

Crystal structure and the pinning mechanisms of the superconducting material are the same in both strand types. Thus, the difference in the scaling behaviour can only be caused by the different strand layout due to the particular manufacturing process.

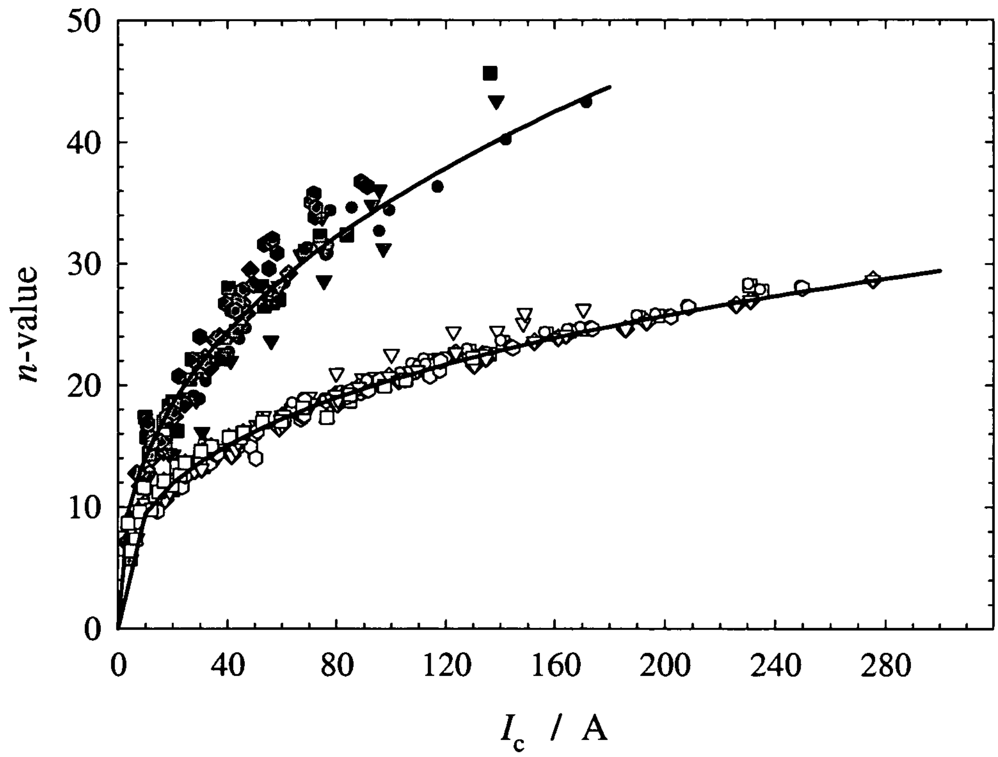

Figure 15: Scaling of the n-values for EM (open symbols) and VAC (full symbols) strands.

4.3 Analysis of U-I-characteristics of a Bi-2223 superconductor

4.3.1 General remarks on Bi-2223

For more than ten years $Bi_2Sr_2Ca_2Cu_3O_{10}$ (Bi-2223, BSCCO-2223) powder-in-tube tapes have experienced a continuous increase in performance. The critical current densities in the high temperature superconductor (HTS) filaments were raised up to $j_c(0\ \mathrm{T},\ 77\ \mathrm{K}) \approx 70\ \mathrm{kAcm^{-2}}$ in short samples

([Mal99]). A better understanding of the mechanical deformation process ([Han97]) and of the Bi-2223 phase development during thermal annealing ([Thu97]) helped to establish a production of some 10 km of such tape conductors with an engineering current density $J_{eng}(0\ \mathrm{T}, 77\ \mathrm{K}) \approx 15\ \mathrm{kAcm}^{-2}$ at a total conductor cross sectional area of $\approx 1\ \mathrm{mm}^2$ ([Fis01], [Fuj02], [Kel02]). Locally, $j_c(0\ \mathrm{T}, 77\ \mathrm{K})$ up to 180 kAcm^{-2} has been observed ([Pol01]), but this seems to be the upper limit for Bi-2223/Ag tapes ([Gra97b]). The reason for this limit are non-superconducting inclusions and pores in the HTS filaments, leading to a percolative supercurrent flow along the Bi-2223 grains, which are well connected, but make up at most only $\approx \frac{2}{3}$ of the filament cross-sectional area ([Dha97]). With an HTS filling factor of high-j_c Bi-2223 conductors of at most 35 %, an intrinsic limit of $J_{eng}(0\ \mathrm{T}, 77\ \mathrm{K}) \approx 60\ \mathrm{kAcm}^{-2}$ has to be expected. This is still comparable to the limit of $\approx 100\ \mathrm{kAcm}^{-2}$ estimated for YBCO ($YBa_2Cu_3O_7$) coated conductors (assuming a future development of $j_c(0\ \mathrm{T}, 77\ \mathrm{K}) \approx 1\ \mathrm{MAcm}^{-2}$ in 5 μm thick YBCO coatings on 50 μm thick metal carrier tapes).

For applications in higher magnetic fields a substantially lower operating temperature is required, however, with the additional benefit of a j_c-increase of up to a factor of 7 compared to 77 K ($j_c(T, 0\ \mathrm{T}) \gg j_c(77\ \mathrm{K}, 0\ \mathrm{T})$, [Kan99]). Another economical disadvantage with respect to YBCO coated conductors is the mandatory use of silver as a matrix material. Previous cost estimations of 10 $\$\mathrm{kA}^{-1}\mathrm{m}^{-1}$ for full-scale production levels ([Mal99]; at present: 200 .. 300 $\$\mathrm{kA}^{-1}\mathrm{m}^{-1}$) have turned out to be too optimistic and are meanwhile adjusted to 25 .. 50 $\$\mathrm{kA}^{-1}\mathrm{m}^{-1}$ for 2006. Moreover, while the good electrical contact of the HTS filaments with the silver matrix is helpful in bridging disconnected HTS regions by means of low resistance shorts ([Pol97]), a frequent use of this current rerouting prevents persistent-mode operation of Bi-2223 coils.

Bi-2223 conductors have overcome many problems on the way to a technical HTS material. The problem of the softness of the silver matrix has been solved by applying dispersed MgO in the silver matrix or by adding a thin layer of stainless steel reinforcement to both sides of the tapes, which enables the tapes to withstand a tensile stress of 300 MPa and a tensile strain of 0.45 % at 77 K ([Mas01]). Promising approaches have been developed to tackle the problem of AC losses, which arise from electromagnetic coupling of the HTS filaments ([Däu98], [Göm97]) and are of concern for all power applications since they determine the necessary cooling power ([Oom00], [Sug97], and [Yam01]): Insulating $BaZrO_3$ ([Hua98]) or $SrCO_3$ barriers ([Eck98]) around the HTS filaments and higher resistive silver alloys such as AgAu or AgPd as a matrix material, as well as twisting of the filaments (down to twist pitches $l_p \approx 1$ cm) reduce these coupling currents. A novel wire arrangement of horizontal and vertical stacks of Bi-2223 tapes reduces the I_c-anisotropy with respect to the orientation of an external magnetic field ([Gra97a]).

In conclusion, Bi-2223 conductors have arrived at a practical level of technical applicability, however, still at a quite high cost level. At present, the biggest psychological handicap for Bi-HTS conductors are the great expectations for a soon arrival of a cheaper and better YBCO coated conductor.

The superconducting Bi-2223 tape examined within the scope of this dissertation was produced by Innova Superconductor Technology Co., Ltd. (InnoST). Currently, this company is a leader in the high temperature superconductor industry in China, its work being focussed on HTS wire production and its applications. The Beijing facility, completed by the end of 2001, gives the company a total production capacity of 200 km of BSCCO-2223 high temperature superconducting wire per year. The production line is fully operational, and sales of HTS wire have already been made both on the domestic and international markets. InnoST plans to expand its production capacity further to 500 km per year by 2004 ([Inn04]).

4.3.2 U-I-measurements on a Bi-2223 tape

Voltage-current characteristics were measured on an InnoST BSCCO-2223 multifilamentary tape. The most important tape specifications are given in table 5.

Table 5: Specifications of an InnoST Bi-2223 multifilamentary tape.

tape width	4.2 mm
tape thickness	0.25 mm
sample length	50 mm
T_c	110 K
I_c(0 T, 77 K)	85 A

All measurements were performed on a short sample of 5 cm length, with a distance between the voltage taps of 1 cm. The orientation of the sample was chosen in a way that the external magnetic field was parallel to the ab-plane of the tape ($B \parallel ab$). The voltage criterion for the evaluation of the measured characteristics is 5 μVcm^{-1}. U-I-curves were recorded in a magnetic field range of $0\ \mathrm{T} \leq B \leq 5\ \mathrm{T}$ and in the temperature range from 10 K to

50 K. By fitting the measured data using the power law from equation 4, the critical currents as well as the n-values were obtained. Some of the measured characteristics are shown in figure 16; the associated parameters are listed in table 6.

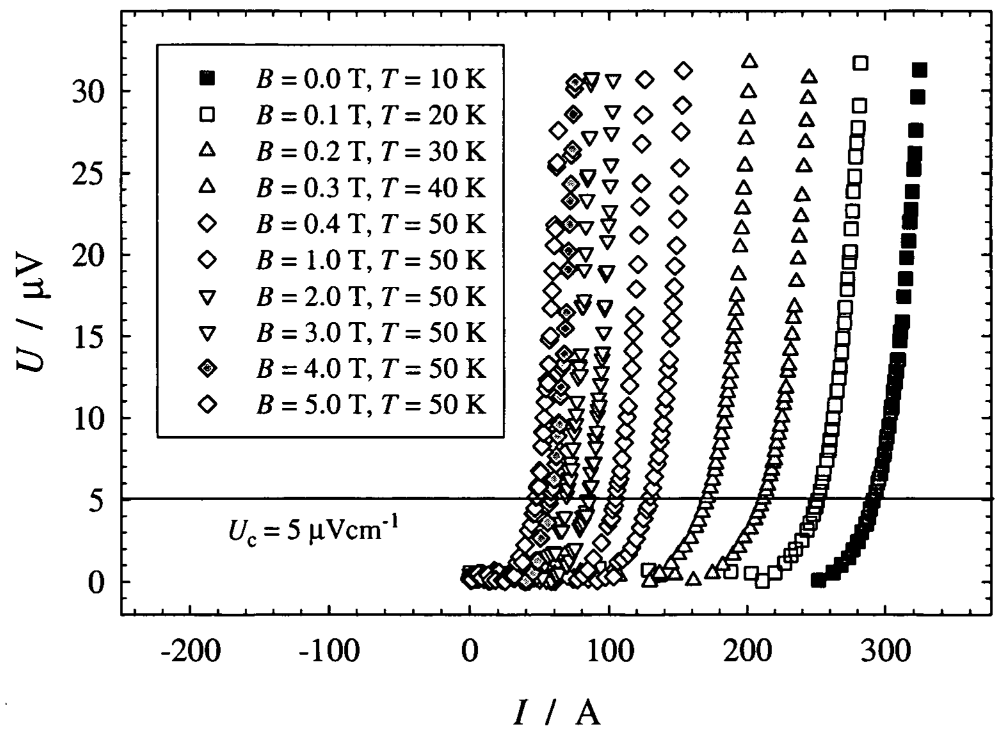

Figure 16: Voltage-current characteristics of Bi-2223 multifilamentary tape for several magnetic fields and temperatures.

It is an interesting task to investigate, whether in case of Bi-2223 the n-value is a function of critical current, too, and, if so, whether the scaling law is similar to the scaling law found for Nb_3Sn superconductors. For this reason, the n-values of all measured curves are plotted versus the critical current (figure 17). Each point in the figure corresponds to one I_c-measurement.

Table 6: Critical currents I_c and n-values for the measurements shown in figure 16.

B / T	T / K	I_c / A	n-value
0.0	10	266	17.5
0.1	20	266	15.3
0.2	30	183	11.4
0.3	40	145	10.0
0.4	50	108	9.4
1.0	50	87	9.0
2.0	50	70	8.4
3.0	50	56	7.8
4.0	50	45	6.8
5.0	50	36	5.9

As one easily can see, the exponents n of the voltage-current-characteristics behave as a function of the critical current in a very similar way as the exponents of the U-I-curves obtained by measurement of Nb_3Sn strands do. For the parameters of equation 7 the following values can be given: $b = 1.31$ and $d = 0.42$. The value of b is distinctly lower than the b-values obtained for EM and VAC strands (by more than a factor of three), whereas d is nearly identical to that of VAC-strands. The lower values of b just arise from the fact that the n-values of Bi-2223 are generally lower than those of Nb_3Sn superconductors.

From the evaluation of the measured curves of Nb_3Sn and Bi-2223 superconductors it is evident that there might exist a general scaling law for the exponents n of U-I-characteristics of type-II superconductors. This scaling

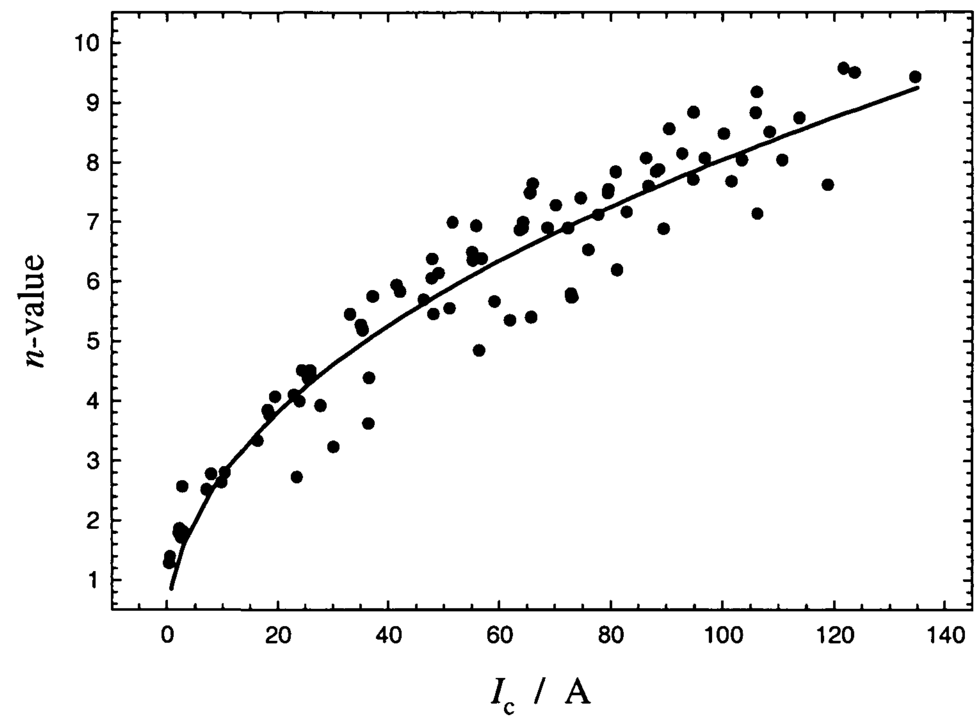

Figure 17: Scaling of the n-value of voltage-current-characteristics of a BSCCO-2223 tape as a function of I_c.

law gives an insight into the flux pinning behaviour close to the transition of the superconductor to normal conductivity (see also subsection 4.1).

It may be assumed that the same or at least a very similar scaling law for $n(I_c)$ can be found for all type-II superconductors being in the Shubnikov state, in which the superconductor is threaded by cylinders of normally conducting material lying parallel to the external magnetic field. These normal cores are arranged in a regular pattern, actually a triangular close-packed lattice ([Ros78]), and responsible for flux pinning in a type-II-superconductor.

4.4 Analysis of U-I-characteristics of lead

Investigations of voltage-current-characteristics as well as the scaling behaviour of the exponents n of those characteristics, which were mentioned in the previous subsections, have shown that there exists a universal scaling law for the n-values as a function of the critical current at least for type-II-superconductors, where flux pinning mechanisms are responsible for their high critical currents and upper critical magnetic fields B_{c2}.

It is therefore of particular interest to investigate, whether any scaling law can also be found for type-I-superconductors, where the external magnetic field is screened from the inner part of the superconducting material by superconducting currents flowing on the surface of the superconductor.

For this reason voltage-current-characteristics were measured on a sample of pure lead with the following geometry: from a lead sheet of 5 mm thickness a cuboid-shaped sample with 3 mm width and 45 mm length was sawn. This short sample was analysed with respect to its purity by scanning electron microscopy (SEM, see subsection 2.4). The spectrum obtained from energy dispersive x-ray spectrometry (EDXRS) showed that the impurities were less than 2 % of the analysed material. A second and at the same time very much convincing proof of the high purity of the lead sample was given by measurement of the critical temperature: $T_c(B{=}0\ \mathrm{T}) = 7.2$ K. This is in accordance with the critical temperature of lead given in the literature (e.g. in [Web79]).

Measurements of voltage-current-characteristics were carried out in a temperature range from 2.75 K to 6 K and in a magnetic field range from 0 T to 100 mT.

From those measurements a critical magnetic field of $B_c(T{=}4.2\ \mathrm{K}) \approx 50$ mT was obtained.

This is in good agreement with the value of $B_c(T=4.2\text{ K}) = 55$ mT given in [Ros78]. The measured U-I-curves were evaluated using a voltage criterion of $U_c = 1\ \mu\text{Vcm}^{-1}$.

In figure 18 some of the measured voltage-current-characteristics are plotted. The I_c- and n-values appendant to those curves are given in table 7. The critical currents and exponents n are again obtained by fitting the measured characteristics using the power law of equation 4.

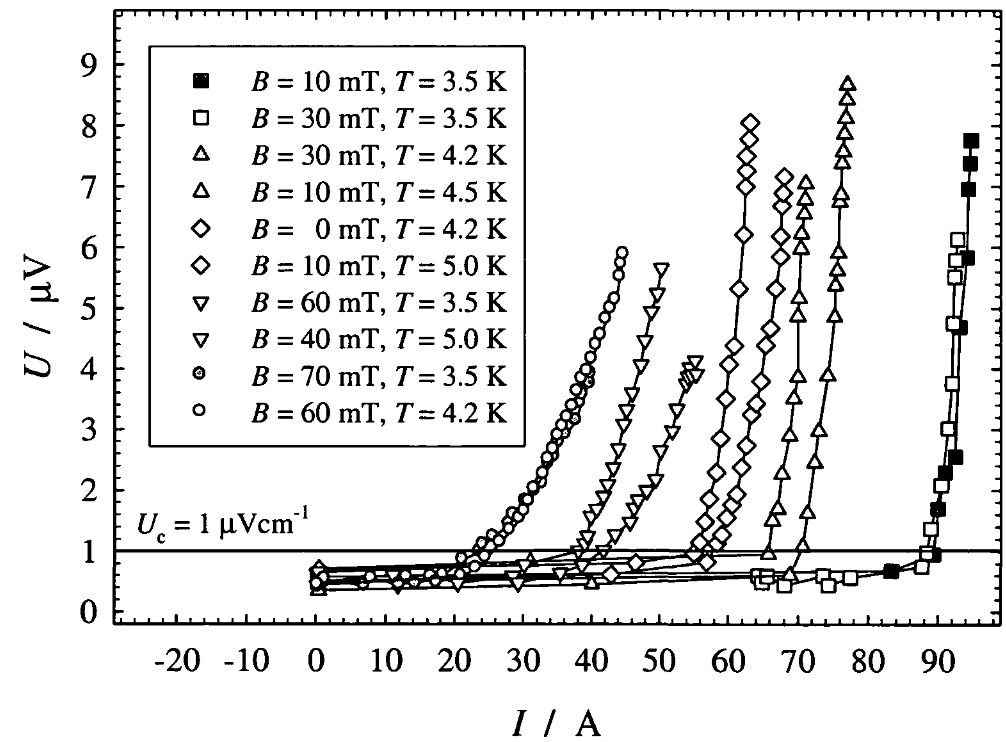

Figure 18: Voltage-current characteristics of a short lead sample for several magnetic fields and temperatures.

In figure 19 the behaviour of the n-values as a function of critical current is displayed. Each point in the plot corresponds to one single measurement.

Obviously, the n-values are scaling with the critical currents also in this type of superconductor, but on the contrary to the findings made upon Nb_3Sn and Bi-2223, the scaling law is completely different. Fitting the n-values gained for lead to the associated critical currents due to equation 7 delivers the following parameters: $b = 0.01$ and $d = 1.95$. Instead of a square root-like scaling law with $d = 0.5$ (typical values of d are close to 0.5 in case of Nb_3Sn and Bi-2223) an almost quadratic increase of the exponents n can be observed for lead. This gives rise to the following general assumption: for

Table 7: Critical currents I_c and n-values for the measurements shown in figure 18.

B / mT	T / K	I_c / A	n-value
10	3.5	89.1	33.2
30	3.5	88.2	33.6
30	4.2	70.1	23.4
10	4.5	65.5	23.0
0	4.2	56.9	11.5
10	5.0	55.2	15.7
60	3.5	40.2	4.1
40	5.0	35.9	5.1
60	4.2	24.4	2.7
70	3.5	22.2	2.1

type-II-superconductors the power d in equation 7 is less than one, whereas $d > 1$ for all type-I-superconductors (maybe actually $d = 2$).

At the moment it is not known, whether this statement, which has been drawn from the analyses of measurement data, can be theoretically confirmed or whether the power d can be theoretically predicted for different superconducting materials, but it is most likely that experiments on other type-I- as well as type-II-superconductors could affirm this assertion. It has to be mentioned that performing experiments on other type-I-superconductors besides lead is not easy, since in the majority of cases their transition temperatures T_c are very low, and so are their critical magnetic fields B_c.

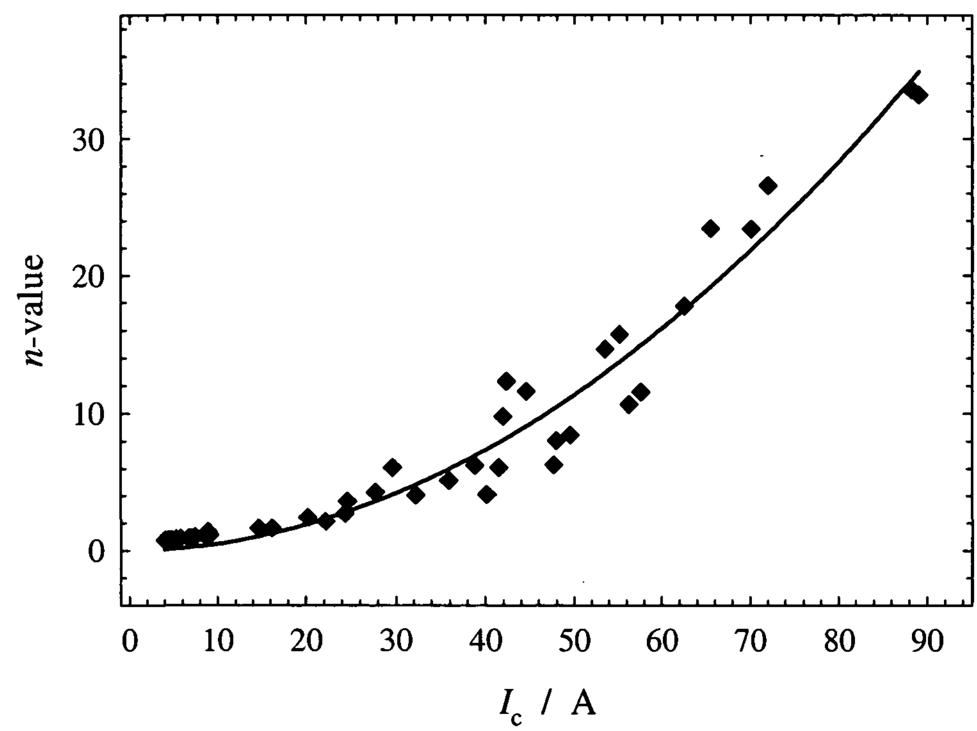

Figure 19: Scaling of the n-value of voltage-current-characteristics of a lead sample as a function of I_c.

It is difficult therefore to carry out measurements over a wide range of temperature or magnetic field, which would be necessary for having enough data to analyse the scaling behaviour of the exponents n over a wide critical current range and thus for obtaining reliable results.

Of course, it can very easily be understood qualitatively that a difference in the flux pinning mechanisms between type-I- and type-II-superconductors leads to a completely different transition behaviour of the material. Here means a difference in the flux pinning mechanisms either really different phenomena, which are responsible for flux pinning and differ from one type-II-superconductor to another, or the changeover from type-II- to type-I-superconductivity, where no flux pinning exists at all.

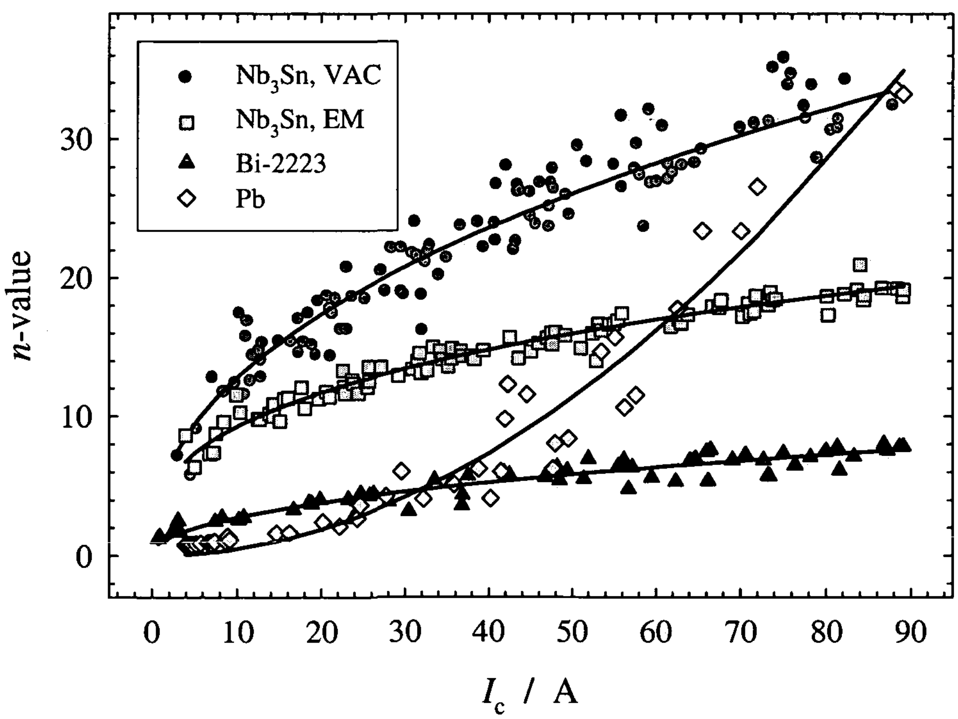

Figure 20: Comparison of the $n(I_c)$ scaling laws for Nb3Sn (EM and VAC), Bi-2223, and Pb.

In figure 20 a comparison of the scaling laws for the n-values as a function of critical current for all superconductors, which were investigated in the scope of this doctoral thesis (Nb_3Sn strands produced by Europa Metalli and Vacuumschmelze, Bi-2223, and lead) is shown. It can be seen very nicely in this figure that for type-II-superconductors the power d in $n(I_c) = b \cdot I_c^d$ is less than one, whereas $d \approx 2$ for lead as a type-I-superconductor. Table 8 lists the parameters b and d obtained from fitting the n-values as a function of critical current using equation 7 for the four superconductors under investigation.

Table 8: Fitting parameters b and d in equation 7 for the different superconductors.

superconductor	b	d
Nb_3Sn (Europa Metalli)	4.11	0.35
Nb_3Sn (Vacuumschmelze)	4.73	0.44
Bi-2223	1.31	0.42
Pb	0.01	1.95

4.5 Scaling behaviour for the exponents of voltage-magnetic field- and voltage-temperature-characteristics of Nb_3Sn strands

Voltage-magnetic field- (U-B-) as well as voltage-temperature- (U-T-) characteristics were measured on the same types of Nb_3Sn strands (EM and VAC) as it was done in the course of the investigation of the scaling behaviour of the exponents of voltage-current-characteristics as a function of critical current, described in the previous subsections.

It will be shown that the data obtained from B_c- and T_c-measurements be fitted using a power law, too. The exponents gained from a fit of those data with a power law are scaling as a function of the critical parameters B_c and T_c respectively. Within some limitations, this scaling is independent of the heat treatment conditions, but it depends on the strand type and the superconducting material under consideration.

In the figures 21 and 22 some of the measured voltage-magnetic field- as well as voltage-temperature-characteristics are displayed for EM- and VAC-

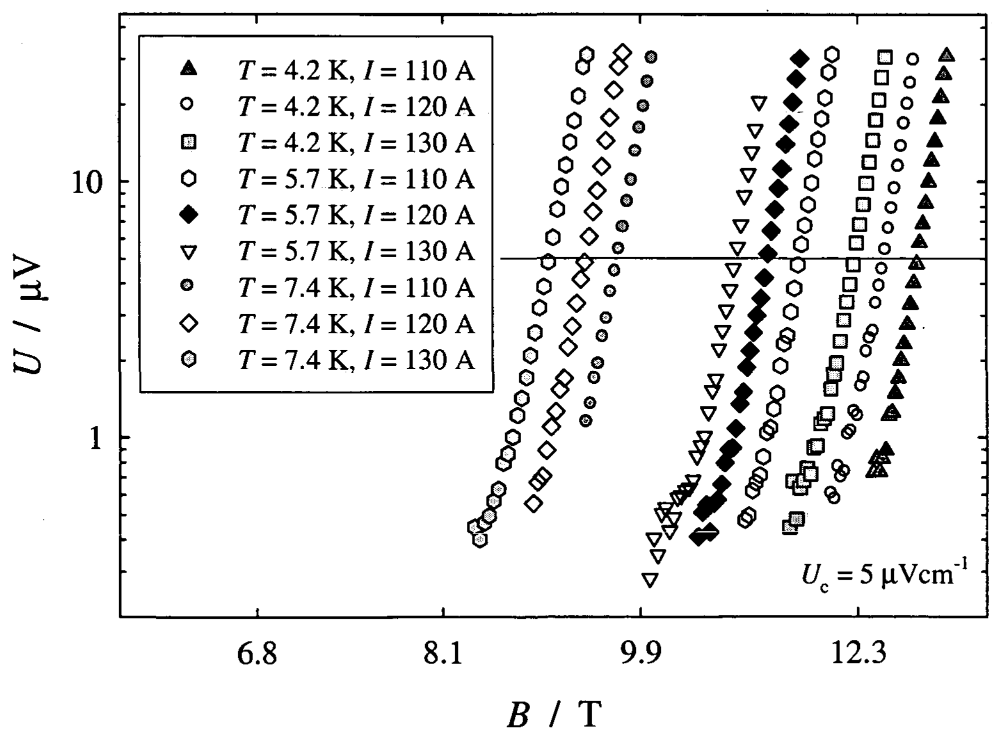

Figure 21: Double-logarithmic plot of the voltage-magnetic field-behaviour of Nb_3Sn. Due to the linear slope of the curves the data can be fitted using equation 8.

Nb_3Sn strands heat treated with the optimised and unified cycle (see subsection 2.4), but for several different durations up to 150 h at 670 °C.
Since in a double-logarithmic scale the measurement data have linear slopes, they can be fitted satisfactorily using a power law similar to equation 4, which has been commonly accepted for the evaluation of I_c-measurement data:

$$U(B) = k_{(\mathrm{B})} B^{o} \quad \text{and} \tag{8}$$

$$U(T) = k_{(\mathrm{T})} T^{m}, \tag{9}$$

where $k_{(\mathrm{B})}$ and $k_{(\mathrm{T})}$, as well as the exponents o and m are fitting parameters. Scaling was shown in subsection 4.2 for the n-value as a function of the critical current. In order to show that the exponents o and m also scale as a function of the critical magnitudes B_c and T_c respectively, several U-B- and U-T-curves were recorded. Figures 23 and 24 show the behaviour of the exponents as a function of the associated critical parameters: $o(B_c)$ and $m(T_c)$. The symbols in the figures give the exponents gained by fitting the measured data using equations 8 and 9. Each symbol represents one single measurement.
For given annealing conditions both the o- and the m-value increase as functions of the critical parameters B_c and T_c. The slopes of the curves displayed in the figures 23 and 24 are nearly identical for all annealing conditions. The absolute values of the exponents, however, depend on the heat treatment conditions. It can be seen from figure 23 that the o-values for the EM samples annealed shorter than 48 h are lying below the o-values of the samples annealed for longer than 48 h. The increase of the exponents can be explained qualitatively by inhomogenities of the Sn-distribution within the

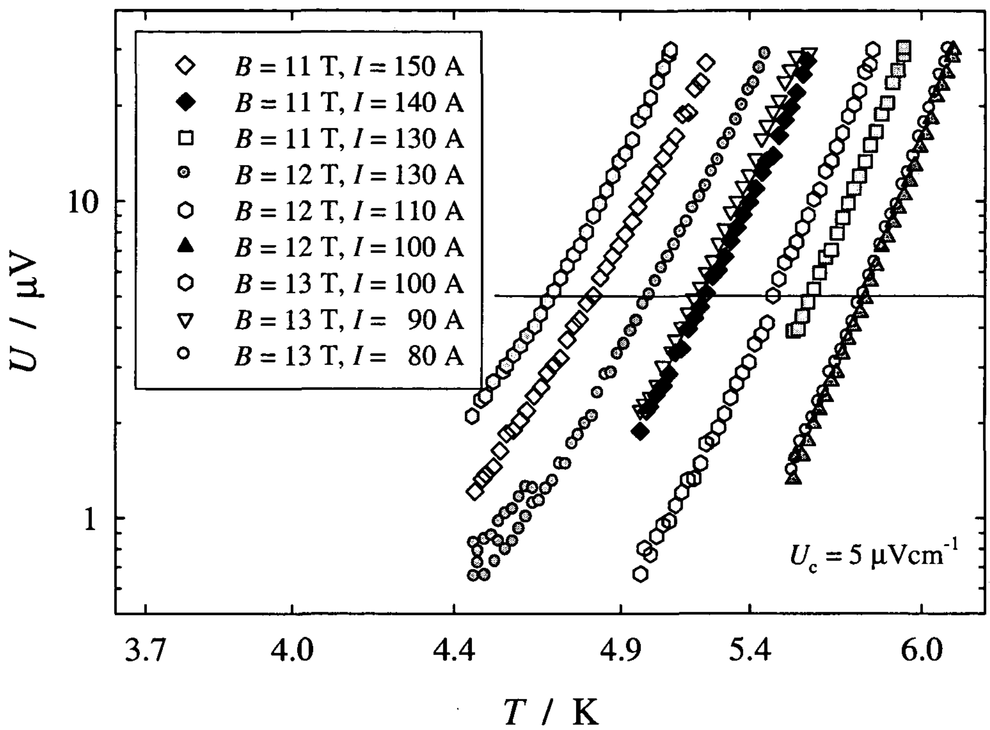

Figure 22: Double-logarithmic plot of the voltage-temperature-behaviour of Nb_3Sn. Due to the linear slope of the curves the data can be fitted using equation 9.

Nb_3Sn filaments ([Lar95]). As B_c is strongly dependent on the chemical decomposition of Nb_3Sn, the resulting spatial variation of B_c results in a drop of the α-values.

For T_c-measurements the influence of the annealing conditions is less than the statistical spread of the data (see figure 24). This is in agreement with the much lower influence of T_c on the annealing conditions ([Fil02a]). No influence of the heat treatment conditions could be found for I_c-measurements by observing the plots of the n-values as a function of non-copper critical

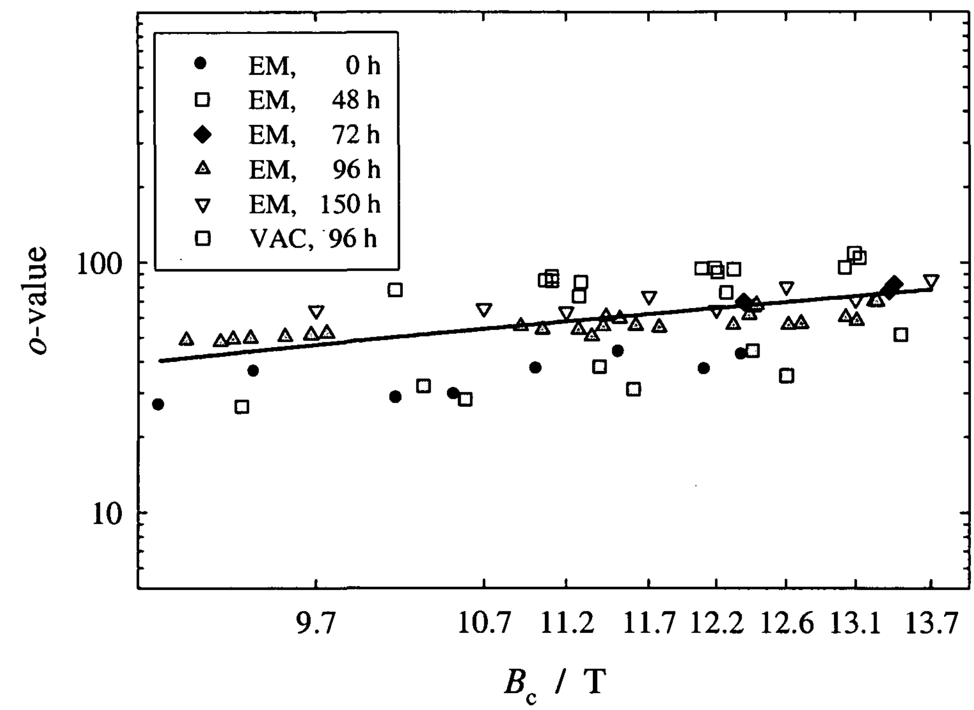

Figure 23: Behaviour of the o-value as a function of the critical magnetic field B_c for EM- and VAC-Nb_3Sn samples annealed for 0 .. 150 h at 670 °C (double-logarithmic plot).

current density ([Fil02b] and [Hen03]). In this case two contrary effects take place:

(1) Longer annealing of the sample leads to an increase of the effective filament diameter and therefore to an increase of that cross section, which carries the superconducting currents. Assuming a constant current density, this results in higher critical currents.

(2) Increasing the average grain size (and simultaneously keeping constant the superconducting cross sectional area) leads to a decrease of the

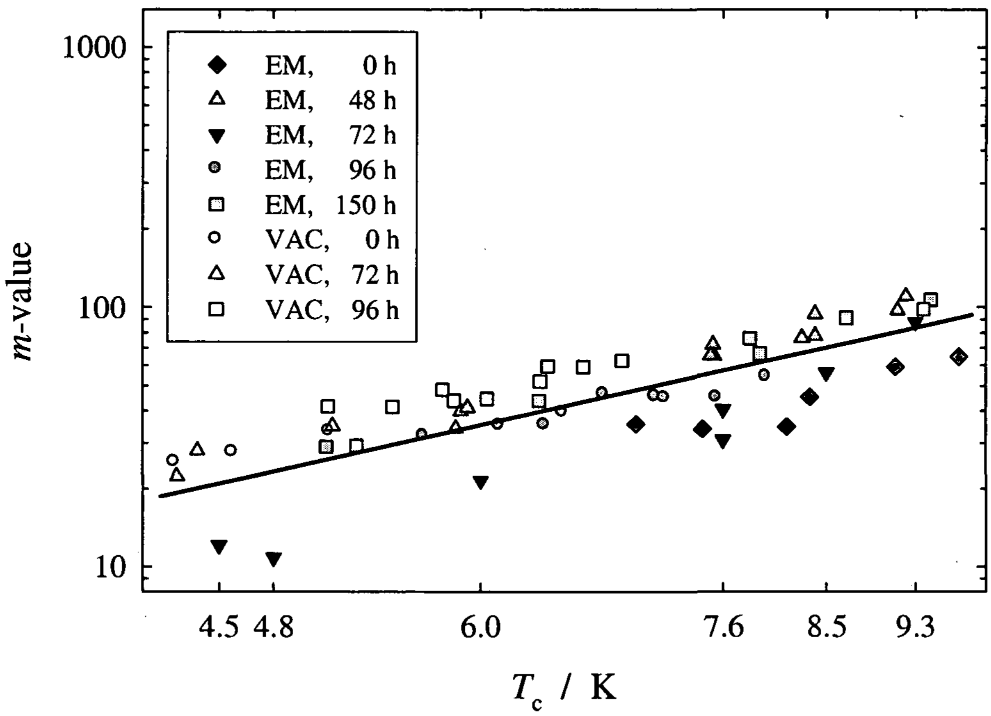

Figure 24: Behaviour of the m-value as a function of the critical temperature T_c for EM- and VAC-Nb_3Sn samples annealed for 0 .. 150 h at 670 °C (double-logarithmic plot).

critical current density ([Lar95]).

Both effects result in a negligible variation of the n-value for all examined annealing conditions.

A similar behaviour as in case of EM internal tin strands can also be found for bronze route strands produced by VAC. The α- and m-values, however, are increased in this case. This increase has also been reported for the n-value ([Ces96]). Since both strand types have been annealed under the same conditions, this change is supposed to arise from the different strand geometry and manufacturing process. In addition, the residual tin content within the filament zone is about four times higher for the EM strand ([Fil01]) compared to the VAC strand having a residual tin content of about 1 %. An additional effect might come from the changed average grain size of the bronze route strand and the internal tin strand. Comparing the grain size distribution given in [Sch81] for bronze route strands to that given in [Kaj02] for internal tin strands, it can be seen that the average grain size of the bronze route strands is about 15 % smaller than the grain size of the internal tin strands.

From a physical point of view the scaling of the exponents o and m obtained from U-B- and U-T-measurements is not well understood at the moment. There exist, however, some promising approaches dealing with the grain size distribution resulting in variations of the pinning force density, critical temperature and upper critical field, but there exist still a lot of unsolved questions in this field.

4.6 Scaling behaviour for the exponents of voltage-magnetic field- and voltage-temperature-characteristics of Bi-2223

Measurements of voltage-magnetic field- as well as voltage-temperature-characteristics were also performed on the Bi-2223 tape described in subsection 4.3.1. U-B-curves were recorded in a temperature range from 10 K to 50 K with transport currents ranging from 60 A to 300 A. Some of the measured characteristics are plotted in figure 25. The curves were fitted using equation 8, with a voltage criterion of $U_c = 2\ \mu\text{Vcm}^{-1}$. The results for critical magnetic fields B_c and the exponents o of those characteristics are given in table 9. Figure 26 shows the behaviour of the o-value as a function of the critical magnetic field. It is evident that the exponent o is nearly constant over the whole field range under observation.

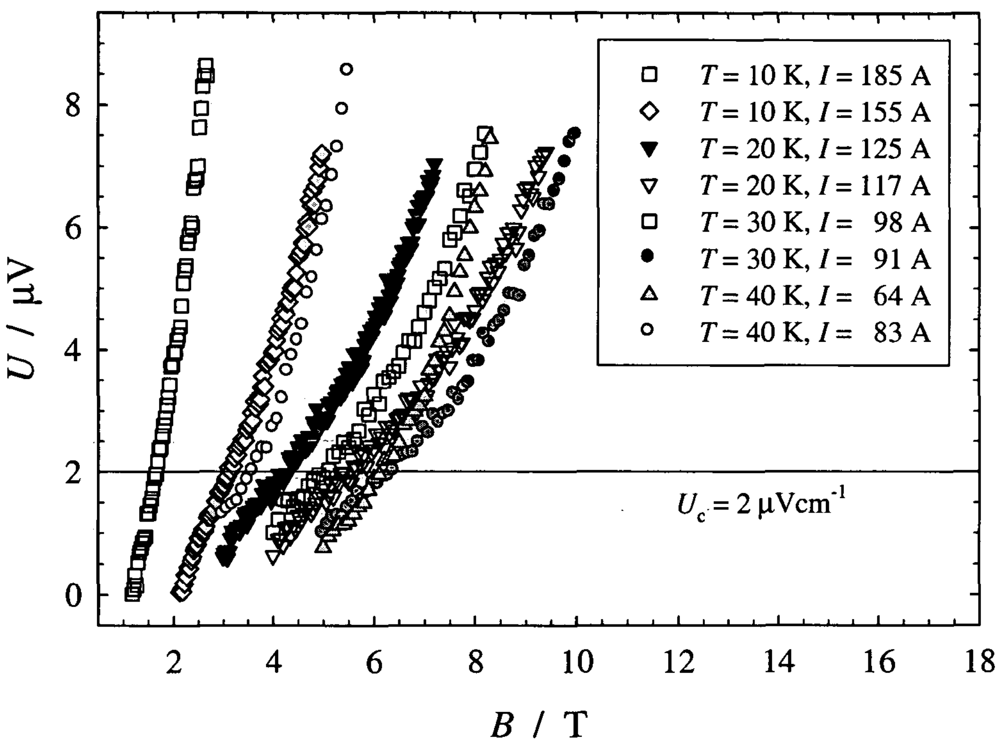

Figure 25: U-B-curves of Bi-2223.

Table 9: Critical magnetic fields B_c and o-values for the measurements shown in figure 25.

T / K	I / A	B_c / T	o-value
30	91	6.4	2.9
40	64	6.2	4.3
20	117	5.6	2.4
30	98	5.1	2.6
20	125	4.2	2.3
40	83	3.6	3.3
10	155	3.1	2.7
10	185	1.6	3.0

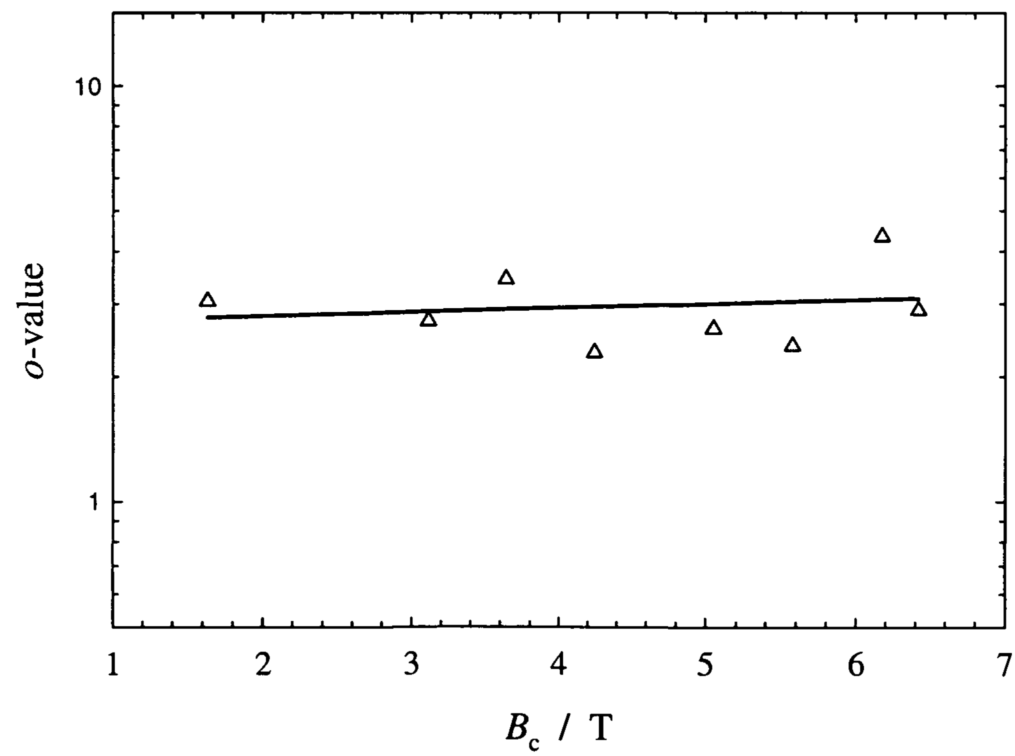

Figure 26: Behaviour of $o(B_c)$ for Bi-2223.

Voltage-temperature-characteristics of the Bi-2223 tape were measured in a field range from 1 T to 5 T, with transport currents between 60 A and 300 A. All measured curves, some of which are displayed in figure 27, have been evaluated according to equation 9. In order to determine the critical temperature, the voltage criterion was chosen to be $U_c = 2\ \mu\text{Vcm}^{-1}$, too. T_c and the m-values for the measurements depicted in figure 27 are listed in table 10. The scaling behaviour of the m-value as a function of T_c is shown

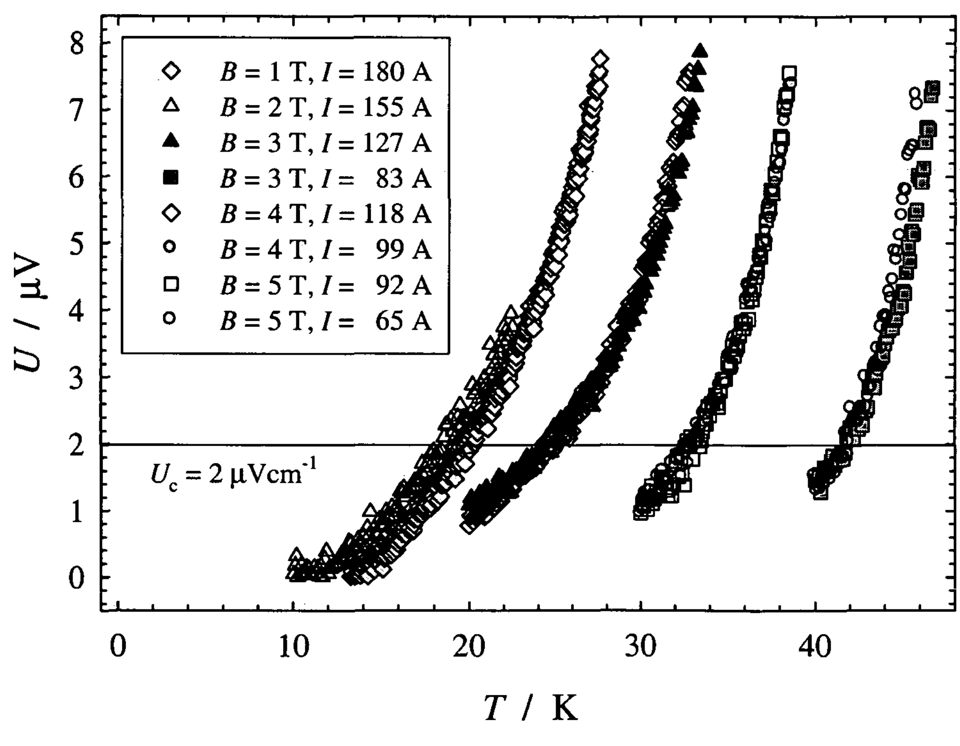

Figure 27: U-T-curves of Bi-2223.

in figure 28. Contrary to the scaling behaviour of $o(B_c)$, a linear increase of the m-value as a function of the critical temperature is clearly observed.

Table 10: Critical temperatures T_c and m-values for the measurements shown in figure 27.

B / T	I / A	T_c / K	m-value
5	65	42.0	13.9
3	83	41.9	11.4
5	92	33.3	8.7
4	99	33.1	8.2
4	118	25.2	4.7
3	127	24.8	4.2
1	180	19.9	3.9
2	155	18.7	3.4

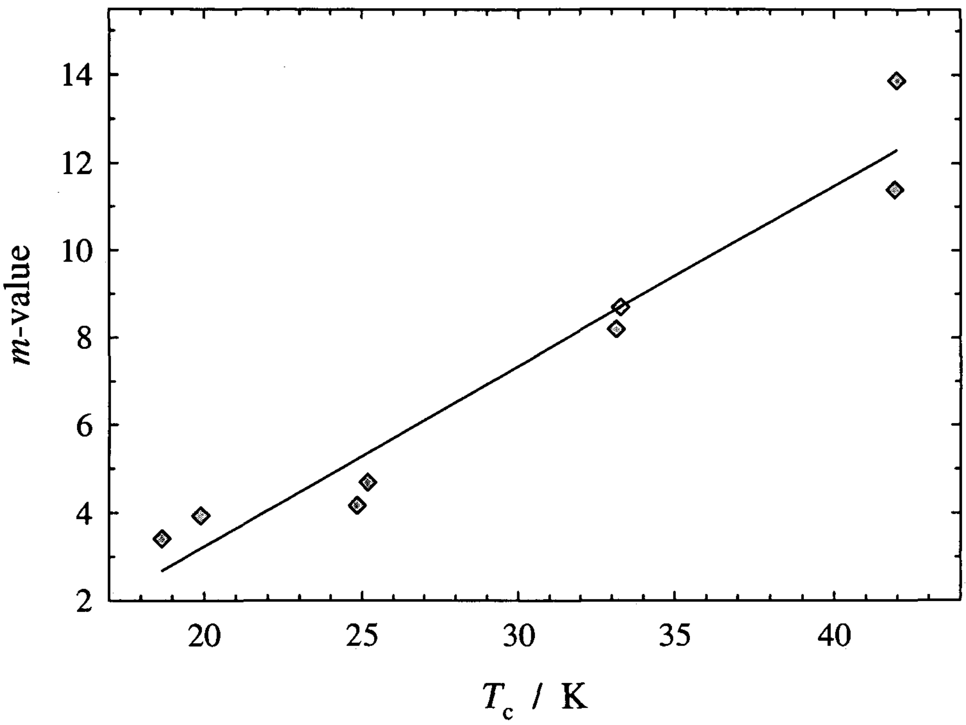

Figure 28: Behaviour of $m(T_c)$ for Bi-2223.

4.7 Scaling behaviour for the exponents of voltage-magnetic field- and voltage-temperature-characteristics of lead

Finallay, voltage-magnetic field- and voltage-temperature-characteristics were examined on the lead sample mentioned in subsection 4.4. On the following pages the results of these investigations are presented:

1. figure 29: some of the measured U-B-curves,
2. table 11: B_c- and o-values for the measurements shown in figure 29,
3. figure 30: scaling behaviour of the o-values as a function of critical magnetic field,
4. figure 31: some of the measured U-T-curves,
5. table 12: T_c- and m-values for the measurements shown in figure 31, and
6. figure 32: scaling behaviour of the m-values as a function of critical temperature.

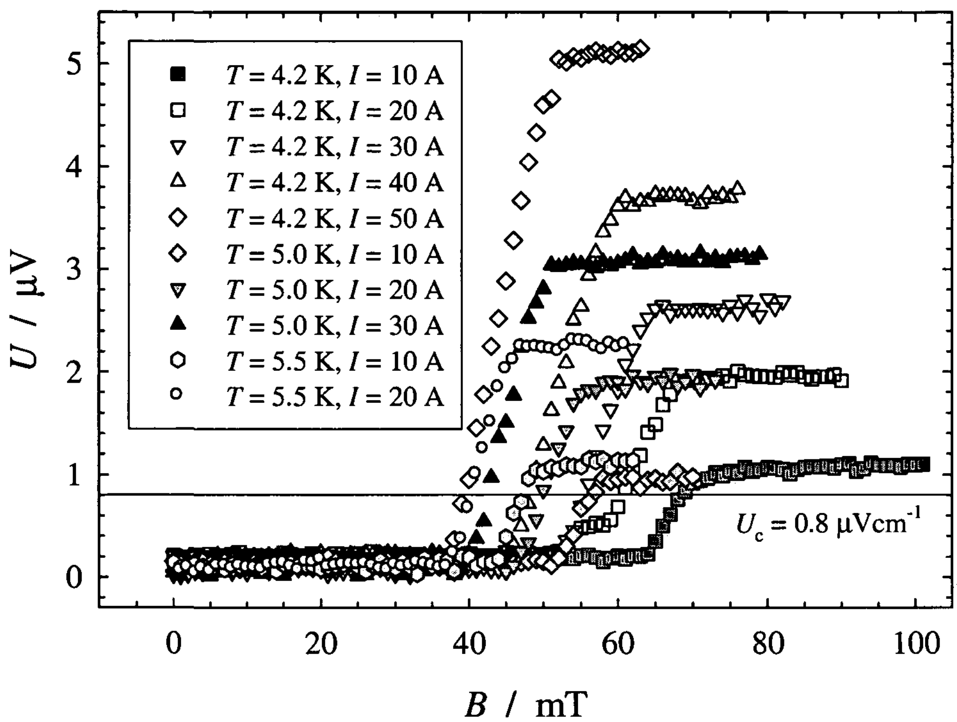

Figure 29: U-B-curves of lead.

Table 11: Critical magnetic fields B_c and o-values for the measurements shown in figure 29.

T / K	I / A	B_c / mT	o-value
4.2	10	69	12.7
4.2	20	60	7.9
5.0	10	57	12.9
4.2	30	56	9.5
5.0	20	51	12.8
4.2	40	48	9.1
5.0	30	43	11.1
5.5	20	41	12.8
4.2	50	38	7.2
5.5	10	34	7.2

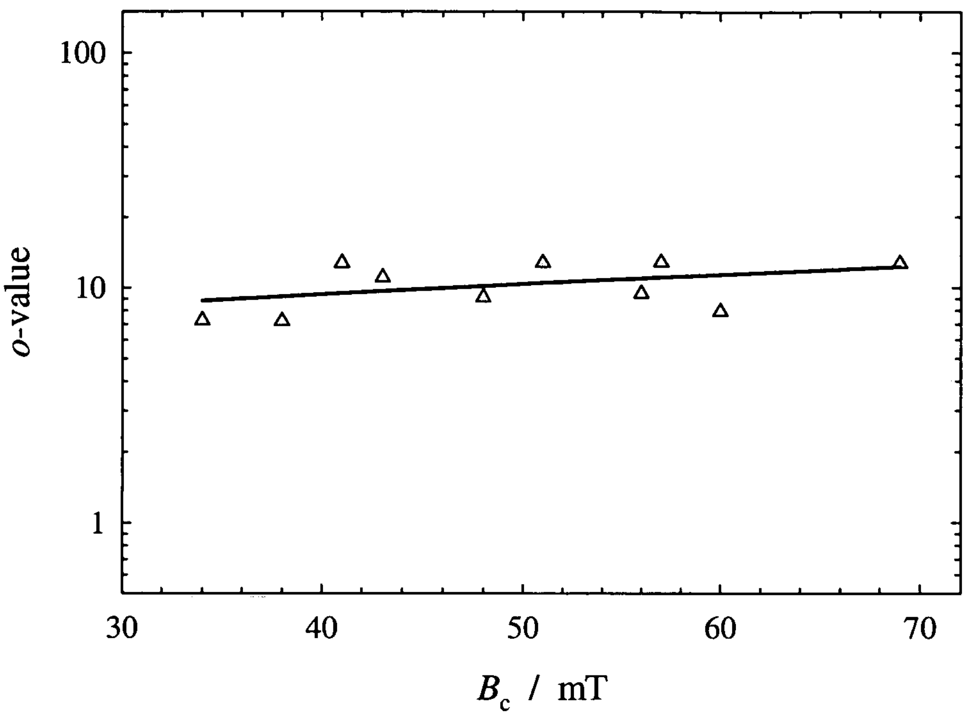

Figure 30: Behaviour of $o(B_c)$ for lead.

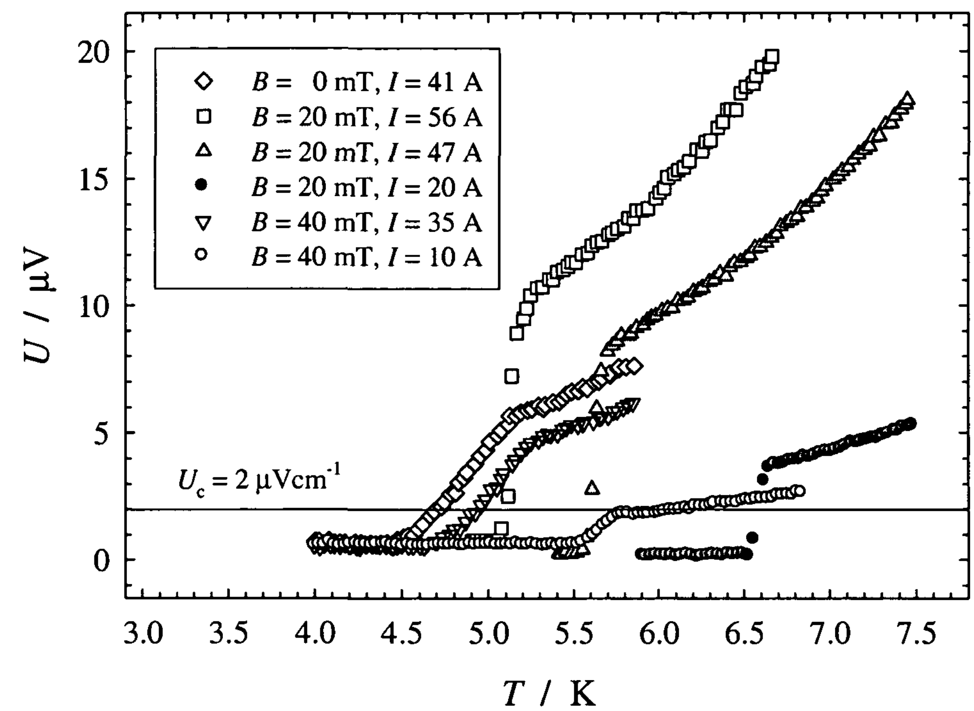

Figure 31: U-T-curves of lead.

Table 12: Critical temperatures T_c and m-values for the measurements shown in figure 31.

B / mT	I / A	T_c / K	m-value
40	10	5.8	23.0
20	47	5.6	103.0
20	55	4.8	48.3
40	35	4.9	17.4
0	41	4.7	11.1

Due to the very low resistivity of lead even in the normally conducting state ($\rho = 0.1\ \mu\Omega$cm), it was possible to record voltage-magnetic field- as well as voltage-temperature-characteristics beginning in the low voltage region up to well above B_c and T_c respectively (see figures 29 and 31). For the evaluation of U-B-curves a voltage criterion of $U_c = 0.8\ \mu$Vcm^{-1} had to be chosen to assure that B_c can be determined for all measurements. The voltage-temperature-characteristics were evaluated with a voltage criterion of $U_c = 2\ \mu$Vcm^{-1}.

Very similarly to the results obtained for Bi-2223, the α-value of lead also remains nearly constant as a function of the critical magnetic field (figure 30).

Looking at figure 32, it can be seen that on the one hand the m-values are very high (much higher than those found for Bi-2223, but comparable to the m-values found for Nb_3Sn around 9 K), and on the other hand vary within an order of magnitude in a temperature range of only 1.5 K. Large values of the exponents m are caused by very narrow transitions of the sample from the superconducting state to normal conductivity. The strong scattering of the exponents m arises from the difficulty of fitting the measured data using a

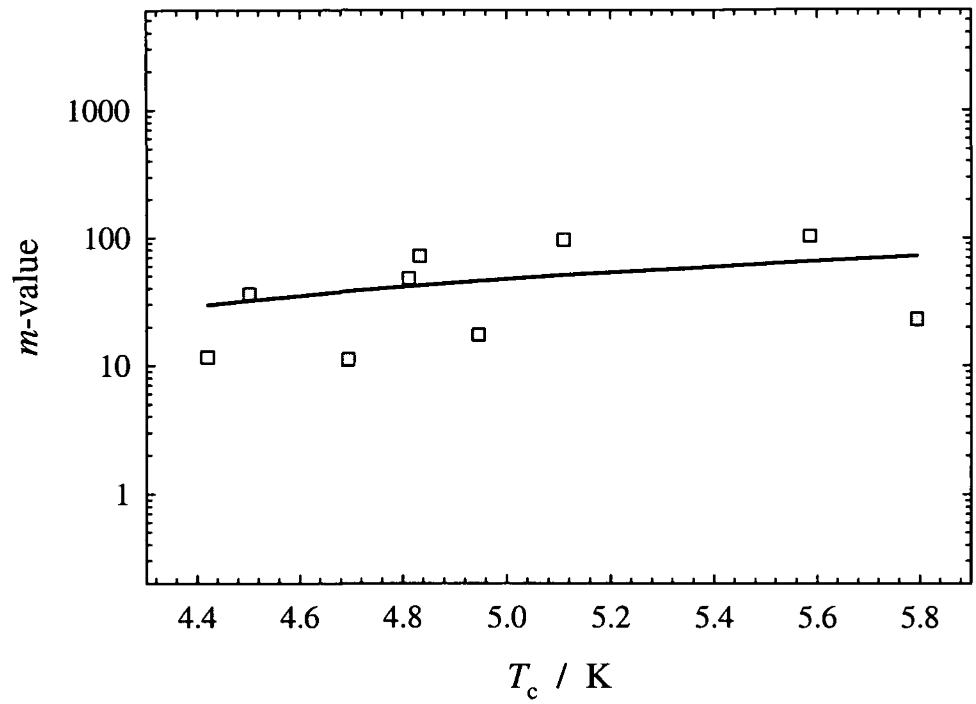

Figure 32: Behaviour of $m(T_c)$ for lead.

power law in the case of very sharp transitions. It has to be kept in mind that the idea of fitting measured curves by a power law arose from investigations of voltage-current-characteristics of Nb_3Sn strands, where the exponents n of the transition characteristics are much lower than the exponents m of the U-T-curves of lead and therefore a power law is much more suitable for data evaluation than it is for the analysis of T_c-characteristics of lead.

As an overview, the functions $o(B_c)$ of all types of superconductors, which were examined in the scope of this dissertation, are compared to each other in figure 33, and so are the functions $m(T_c)$ in figure 34. It can clearly be seen

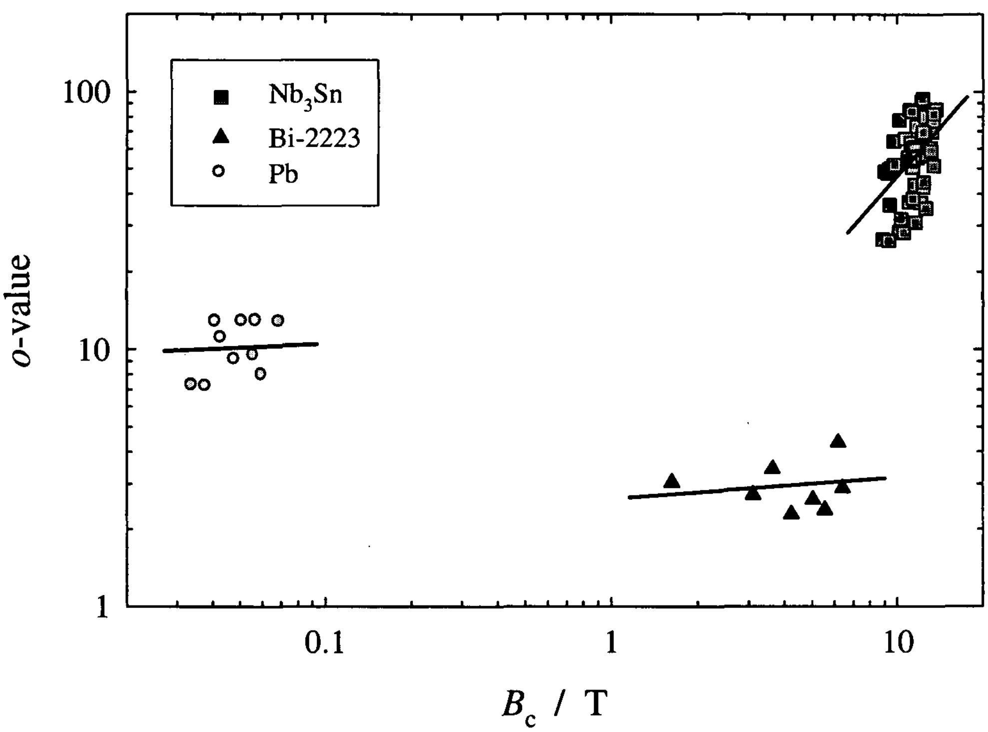

Figure 33: Comparison of the scaling behaviour of $o(B_c)$ of Nb_3Sn, Bi-2223, and Pb.

in figure 33 that the ranges of o-values of the three superconductors are well separated from each other. Furthermore, the figure shows that for Bi-2223 and lead the exponents o nearly stay constant over the whole critical magnetic field range, where measurements were done in, whereas the o-values of Nb_3Sn-strands increase linearly with increasing B_c. Moreover, the exponents o of

Nb_3Sn are higher than those obtained for Bi-2223 or lead by almost one order of magnitude.

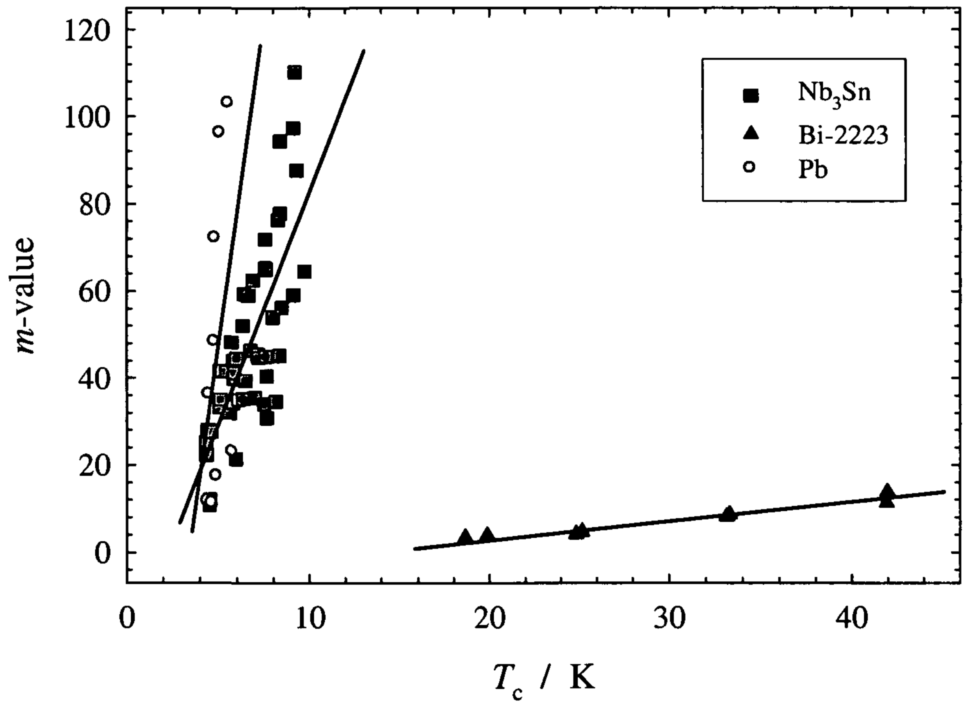

Figure 34: Comparison of the scaling behaviour of $m(T_c)$ of Nb_3Sn, Bi-2223, and Pb.

Figure 34 shows a linear increase with critical temperature of the exponents m of U-T-characteristics for all types of superconductors examined. Nevertheless, it is noteworthy that the slopes of the functions $m(T_c)$ are much steeper for Nb_3Sn and lead than the slope is in $m(T_c)$ for Bi-2223. It also attracts attention that the scaling behaviour of the m-values as a function of critical temperature is similar for Nb_3Sn and lead, the former being a type-I-superconductor, the latter a type-II-superconductor. Finally, it has to be asserted that the m-values gained for Nb_3Sn and lead are distinctly higher than those of Bi-2223 (again by one order of magnitude).

Comparing the type-II-superconductors Nb_3Sn and Bi-2223, both the o- and the m-values are much higher in case of Nb_3Sn. This indicates a distinctly stronger pinning force density in Nb_3Sn.

5 Mathematical model for the calculation of U-I-, U-B-, and U-T-curves of Nb_3Sn

With the knowledge of the grain size distribution of Nb_3Sn in Nb_3Sn superconductors it is possible to draw up a model for the calculation of voltage-current-, voltage-magnetic field-, and voltage-temperature-characteristics. Thus, from the calculated curves the critical parameters I_c, B_c, and T_c and the exponents n, o, and m of these characteristics can be determined.

A detailed explanation of the model will be given below. Calculated curves and values will be compared with those obtained from measurements.

The grain size distribution of Nb_3Sn in a Nb_3Sn strand was reported by P. J. Lee et al. ([Lee00]) to be a log-normal distribution given by equation 10. Equation 11 is the normalisation condition for the distribution function $P(a)$ that allows to calculate the normalisation constant N, taking the parameters given in [Lee00]: the mean grain size $\mu = 134$ nm and the full width at half maximum $\Gamma = 1/\sigma^2 = 77$ nm. For simplification it is assumed that the grains are cubes with side length a. It is also assumed that the critical current of a grain is a function of its size a. This leads to the following distribution function:

$$P(a) = N \exp\left(-\frac{\ln^2\left(\frac{a}{\mu}\right)}{2\sigma^2}\right) = N \exp\left(-\frac{\Gamma}{2}\ln^2\left(\frac{a}{\mu}\right)\right) \qquad (10)$$

$$\int_0^\infty P(a)\,\mathrm{da} = 1 \qquad (11)$$

When a transport current starts to flow through the superconducting material, it is at first too low to suppress superconductivity even in the smallest grains, and no voltage drop can be observed. As the current increases, the smallest grains become normally conducting and contribute to the total voltage drop. By further increasing the transport current, the critical current of the next larger grains is exceeded, and a higher voltage drop occurs. The same happens for the next larger grains and so on. The normalised function $P(a)$ (see equation 10) is proportional to the number of grains with a certain size a and thus accounts for the fact that the voltage drop increases all the more the more grains of a certain size exist. The total voltage drop on the superconductor is obtained by summing up the voltage drops of all grains. These elementary considerations lead to a power law-like voltage-current-characteristic with $U(I) \;\propto\; I^n$.

The critical current I_c of a grain with side length a is given by $I_c \;=\; J_c a^2$, where J_c is the critical current density obtained from Summers' formula ([Sum91], equations 12), and a^2 is the cross sectional area of a (cubic) grain.

$$J_c(B,\,T) \;=\; C_0\; B_{c20}^{-\frac{1}{2}} \left(1-\left(\frac{T}{T_{c0}}\right)^2\right)^2 \left(1-\frac{B}{B_{c2}(T)}\right)^2 \tag{12}$$

$$B_{c2}(T) \;=\; B_{c20}\left(1-\left(\frac{T}{T_{c0}}\right)^2\right)\left[1-0.31\left(\frac{T}{T_{c0}}\right)^2\left(1-1.77\ln\left(\frac{T}{T_{c0}}\right)\right)\right] \tag{13}$$

By fitting the I_c-values, measured as a function of magnetic field B and temperature T, using equations 12 and 13, the Summers-parameters can be determined. For Nb_3Sn they are: $C_0 \;\approx\; 2000$ Amm^{-2}T$^{0.5}$, $T_{c0} = 18$ K, and $B_{c20} = 28$ T.

While in a certain magnetic field B and at a temperature T the critical current *density* J_c is independent of the grain size, the critical *current* I_c sensitively depends upon the grain size.

5.1 Calculation of U-I-curves

Using the considerations made in the previous section, the $U(\tilde{I})$-behaviour of a Nb_3Sn strand at the temperature T and in an external magnetic field B can be calculated:

$$U(\tilde{I}) = \sum_a \tilde{I}\,\Theta\left(\tilde{I} - \alpha f(a)\right) P(a)\, a^3\, g(B,\, T) \tag{14}$$

$$f(a) = \frac{A}{C_0} J_c(B,\, T) a^2 = \frac{A}{C_0} I_c(a) \tag{15}$$

$$g(B,T) \approx 10^{[(63-T)\lg B - 2(41-2\,T)]} \tag{16}$$

$$\alpha = 4\ \mathrm{Amm}^{-4}\mathrm{T}^{0.5} \tag{17}$$

The function $f(a)$ in the argument of the Heaviside function $\Theta\left(\tilde{I} - \alpha f(a)\right)$ accounts for the change of critical currents I_c subject to different grain sizes a. The factor α was determined empirically by comparing calculated and measured U-I-curves, which were taken from a general database for Nb_3Sn strands manufactured by Europa Metalli (EM) and Vacuumschmelze (VAC) respectively. This database has been compiled at Vienna University of Technology, Institute of Solid State Physics, and is containing hundreds of U-I-, U-B-, and U-T-curves. In equation 15 the non-copper cross sectional area of a Nb_3Sn-strand is $A = 0.21\ \mathrm{mm}^2$.

According to Ohm's law the total voltage drop must be $U(\tilde{I}) = \tilde{I}R$ with R the resistance of the normally conducting fraction of Nb_3Sn at the current $\tilde{I}$, which is proportional to the volume a^3 of the grains and their number $P(a)$.

The resistance is given by $R = P(a)\,a^3\,g(B,\,T)$ as a function of grain size, magnetic field, and temperature, where $g(B,\;T)$ was also found empirically by comparing calculated and measured voltage-current-characteristics. Equation 14 yields U-I-curves that can be fitted using a power law of the

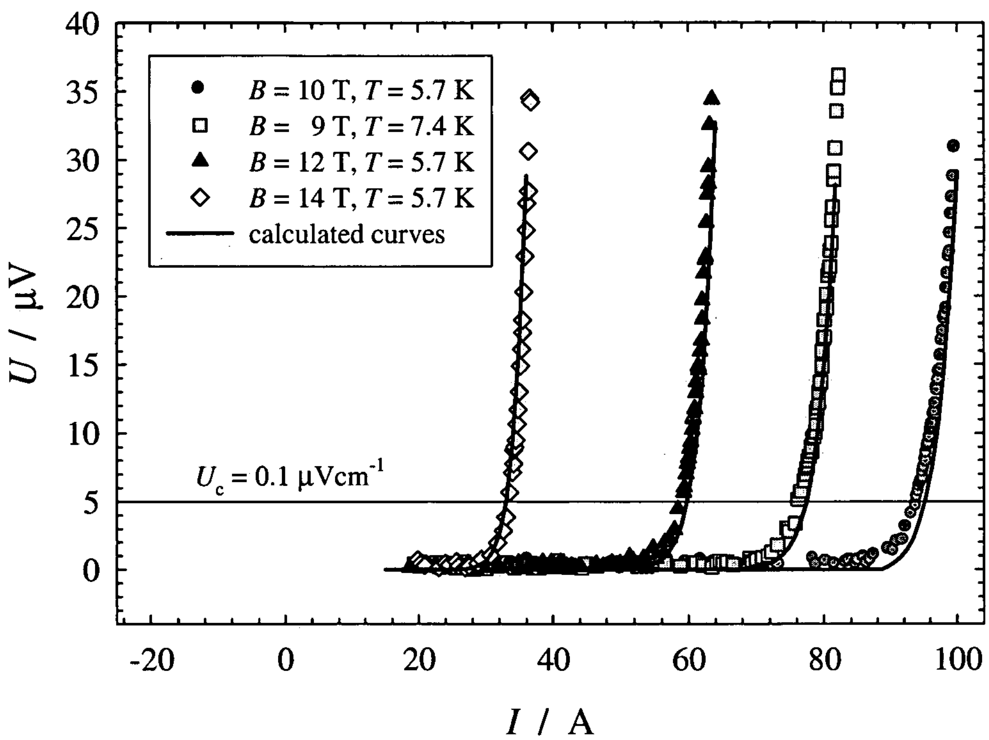

Figure 35: Comparison of calculated and measured U-I-curves for Nb3Sn strands.

well known form $U(\tilde{I}) = k_{(\mathrm{I})}\tilde{I}^n$, and thus the n-value is gained. To obtain the correct I_c-values from the calculated $U(\tilde{I})$-behaviour in accordance with the measured critical currents, it is necessary to rescale the current axis of the calculated curves to $I = \beta\tilde{I}J_\mathrm{c}(B,T)A/C_0$ with $\beta = 2\ \mathrm{mm}^{-2}\mathrm{T}^{0.5}$.

In figure 35 calculated voltage-current-characteristics of Nb3Sn strands produced by both Europa Metalli and Vacuumschmelze are compared to measured curves for different magnetic fields and temperatures. Calculated

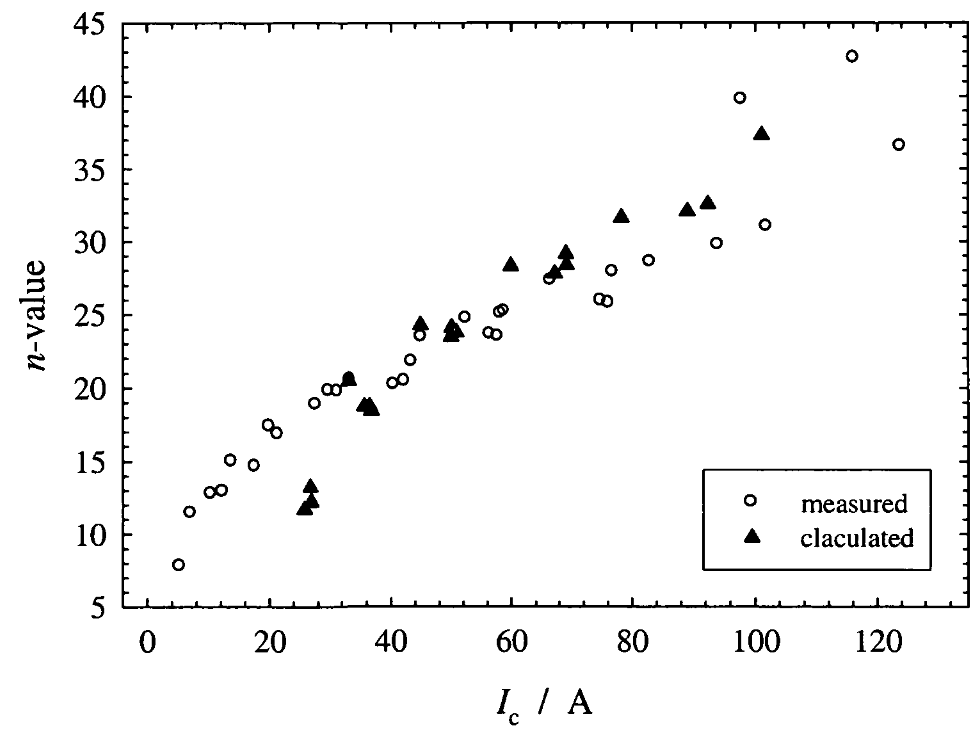

Figure 36: Comparison of calculated and measured n-values for Nb_3Sn strands.

n-values are plotted together with those obtained from measurements in figure 36. From this figure it is obvious that calculation and experiment agree very well with each other.

5.2 Calculation of U-B-curves

For the calculation of voltage-magnetic field-characteristics equation 14 is used in a modified form:

$$U(B) = \sum_a I\,\Theta\,(I - \alpha f(a,B))\,P(a)\,a^3\,g(I,T) \tag{18}$$

In this case temperature T and transport current I are kept constant, whereas the external magnetic field B is varied.

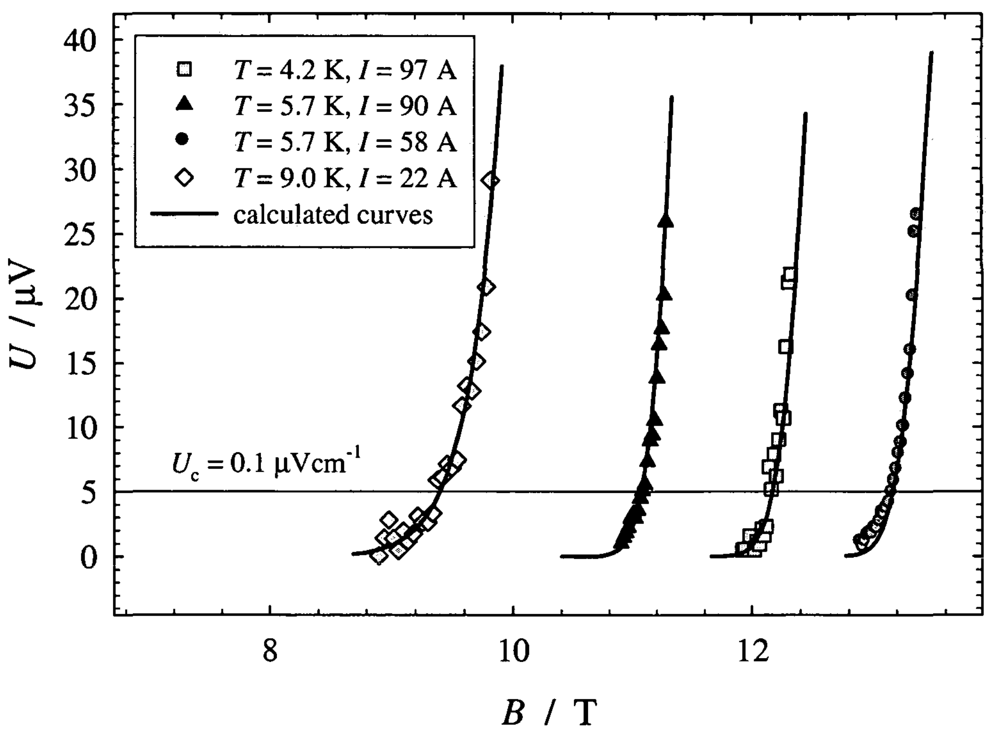

Figure 37: Comparison of calculated and measured U-B-curves for Nb_3Sn strands.

The resistance of the normally conducting fraction of Nb_3Sn in a magnetic field B is now given by $R = P(a)\,a^3\,g(I,\,T)$. The calculated U-B-curves can also be fitted using a power law of the form $U(B) = k_{(\mathrm{B})}B^o$, which delivers the exponent o as well as the critical magnetic fields B_c. Figure 37 shows

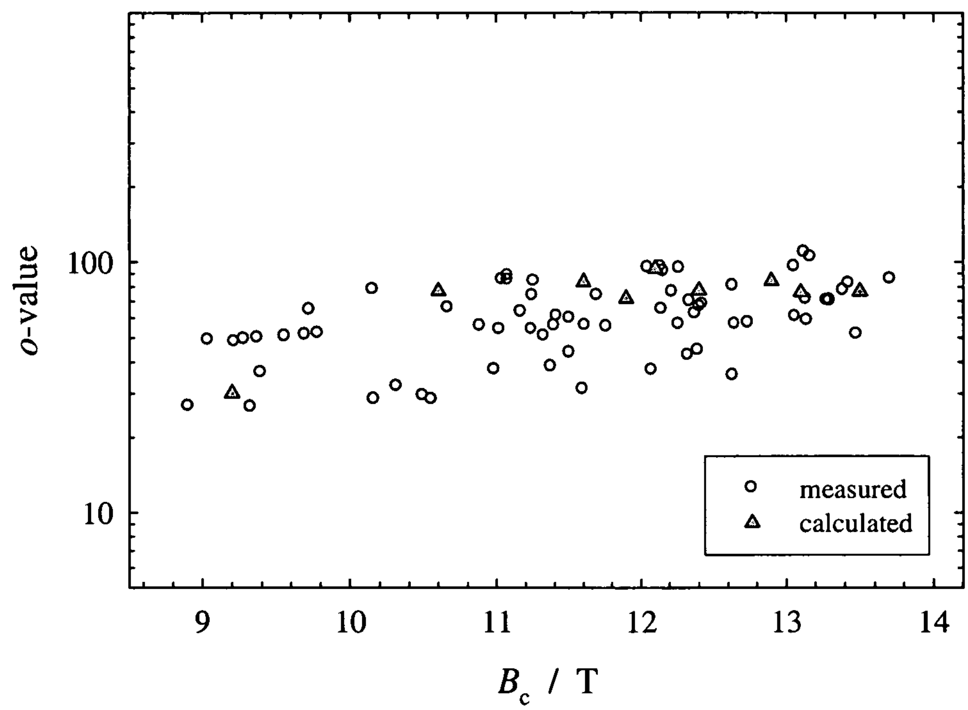

Figure 38: Comparison of calculated and measured o-values for Nb_3Sn strands.

calculated and measured voltage-magnetic field-curves (also taken from the general database mentioned above) for different temperatures T and currents I. A comparison of calculated and measured o-values is illustrated in figure 38, again yielding very good agreement with each other.

5.3 Calculation of U-T-curves

Finally, for the calculation of voltage-temperature-characteristics equation 14 is once more modified, yielding:

$$U(T) \;=\; \sum_a I\,\Theta\,(I - \alpha f(a,T))\,P(a)\,a^3\,g(B,\,I) \tag{19}$$

Now the magnetic field B and the transport current I are kept constant, whereas the temperature T is varied. The resistance of the normally conduct-

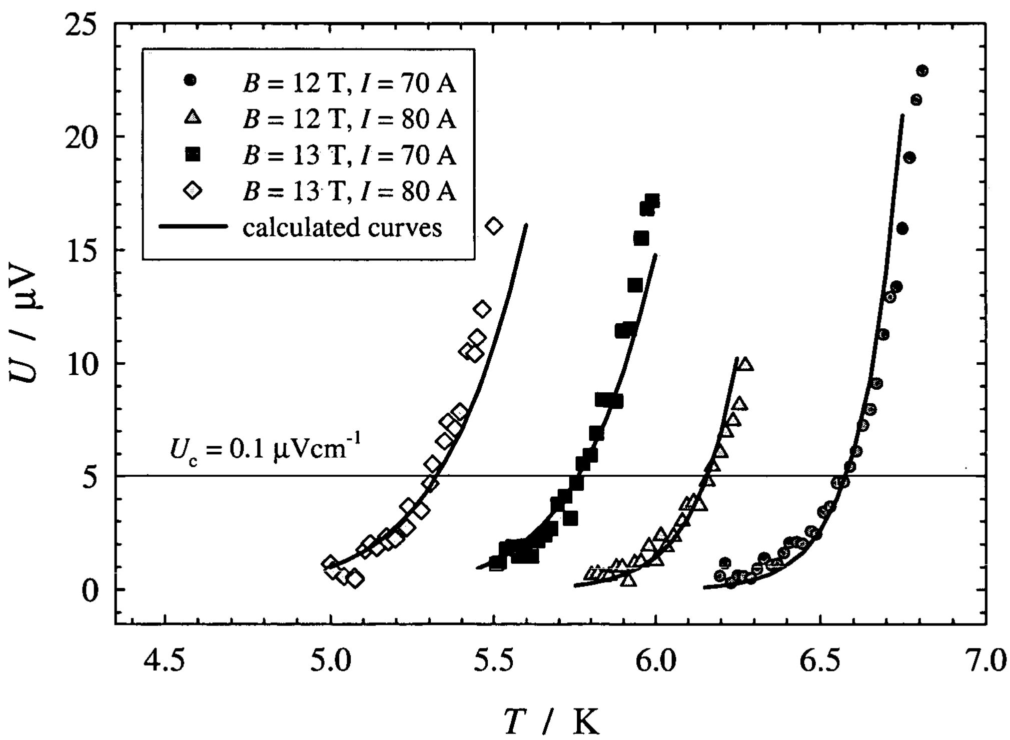

Figure 39: Comparison of calculated and measured U-T-curves for Nb_3Sn strands.

ing fraction of Nb_3Sn at a temperature T is given by $R = P(a)\,a^3\,g(B,\,I)$.

The U-T-curves obtained from the calculation can again be fitted using a power law of the form $U(T) = k_{(T)}T^m$, yielding the m-values as well as the critical temperatures T_c. In figure 39 calculated and measured voltage-

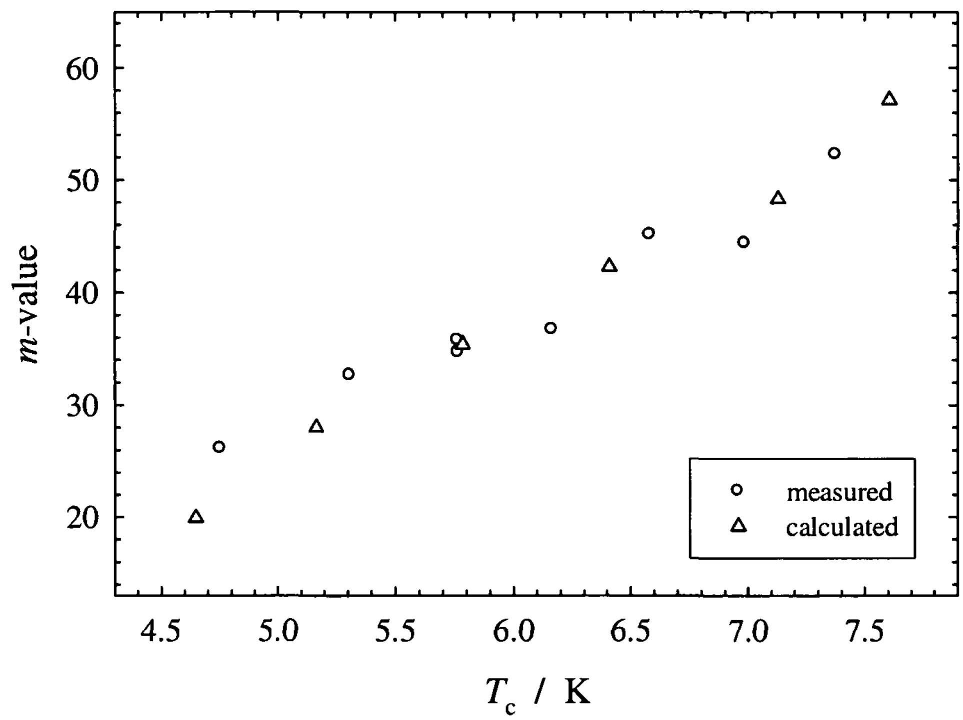

Figure 40: Comparison of calculated and measured m-values for Nb_3Sn strands.

temperature-curves are displayed for different magnetic fields B and currents I. A comparison of calculated and measured m-values is illustrated in figure 40, again yielding a reasonable agreement with each other.

5.4 Summary

It has been shown that, being aware of the grain size distribution function for Nb_3Sn grains and Summers' formula, U-I-, U-B-, and U-T-characteristics can be calculated for Nb_3Sn strands in various magnetic fields and at several temperatures and currents respectively. From those calculations the exponents n, o, and m of the $U(I)$-, $U(B)$-, and $U(T)$-behaviour as well as the critical parameters I_c, B_c, and T_c can be predicted. It was also shown that the calculations are in good agreement with the data experimentally obtained.

Nevertheless, at the moment the presented model is suitable only for Nb_3Sn superconductors, since one of the main elements in the calculations is the functional form of the empirical model, found by Summers ([Sum91]), which allows to calculate the critical current density j_c in multifilamentary Nb_3Sn as a function of magnetic field and temperature. Although within the model worked out in the framework of this doctoral thesis some simplifying assumptions are made, it is evident that this is the right way to mathematically describe the transition from superconductivity to normal conductivity in any superconductor.

As soon as a function is found for the calculation of $j_c(B, T)$ for a given superconducting material, the model described above will be able to yield voltage-current-, voltage-magnetic field-, and voltage temperature-characteristics for this superconductor.

The findings gained by the studies of the model for the prediction of the exponents of U-I- and U-T-characteristics of multifilamentary Nb_3Sn strands will be published in the proceedings of the European Conference on Advanced Superconductivity (EUCAS) 2003.

6 Conclusion

The results gained within the scope of this dissertation can be summarised as follows:

- It was shown for Nb_3Sn strands that a shorter heat treatment than recommended by the manufacturers Europa Metalli and Vacuumschmelze does not negatively affect the performance of the material (critical current I_c, residual resistance ratio RRR, and hysteresis losses Q_0). Instead of 554 hours (EM) or 569 hours (VAC), respectively, the total annealing time can be reduced to 470 hours. Moreover, it was demonstrated that both strand types can be reacted at the same time without worsening the superconducting properties.

- Voltage-current-, voltage-magnetic field-, and voltage-temperature-characteristics were recorded for three different superconductors: Nb_3Sn, Bi-2223, and lead (Pb). It turned out that the curves experimentally obtained could be fitted using a power law. Thus, they were analysed with respect to their critical values (I_c, B_c, and T_c) as well as to the exponents n, o, and m of this power laws.

- For all of the three examined superconducting materials it was shown that the exponents of their transition characteristics are functions of the associated critical values: $n = n(I_c)$, $o = o(B_c)$, and $m = m(T_c)$. A comparison and discussion of the scaling behaviour of the n-, o-, and the m-value is given for all superconductors under investigation.

- Finally, a mathematical model was drawn up, which allows to calculate the power law-like voltage-current-, voltage-magnetic field-, and voltage-temperature-characteristics of Nb_3Sn. Thus, this model is capable of predicting the critical parameters (I_c, B_c, and T_c) and exponents (n, o, and m) of those transition curves. Furthermore, it was shown that the curves and exponents calculated within the frame of this model are in good agreement with the data gained from the measurements.

References

[Bru96] P. Bruzzone, N. Mitchell, M. Steeves, M. Spadoni, Y. Takahashi, and V. E. Sytnikov. Conductor fabrication for the ITER model coils. *IEEE Transactions on Magnetics*, 32(4):2300–2303, July 1996.

[Ces96] L. Cesnak, F. Gömöry, and P. Kováč. Pinning potential, its relativity and dependence on temperature and magnetic field studied on the basis of the *I-V* characteristics of multifilamentary Nb_3Sn superconductors. *Superconductor Science and Technology*, 9:184–191, March 1996.

[Däu98] M. Däumling. AC power loss for superconducting strips of arbitrary thickness in the critical state carrying a transport current. *Superconductor Science and Technology*, 11:590–593, June 1998.

[Dha97] M. Dhallé, M. Cuthbert, M. D. Johnson, J. Everett, R. Flükiger, S. X. Dou, W. Goldacker, T. Beales, and A. D. Caplin. Experimental assessment of the critical current-limiting mechanisms in BSCCO/Ag high-temperature superconducting tapes. *Superconductor Science and Technology*, 10:21–31, January 1997.

[Eck98] H. Eckelmann, M. Däumling, M. Quilitz, and W. Goldacker. AC transport current losses of multifilamentary Bi(2223) tapes with varying filament geometries. *Physica C*, 295:198–208, 1998.

[EFD04] European Fusion Development Agreement.
URL: http://www.efda.org, February 2004.

[Fäh77] M. Fähnle. Zur Theorie der Haftkräfte in Nb_3Sn. Ph.D. thesis, Universität Stuttgart, 1977.

[Fil01] H. Fillunger, M. Foitl, K. Hense, I. Kajgana, H. Kirchmayr, A. Kasztler, C. Kolbeck, I. Kral, and R. Maix. Influence of the heat treatment of internal tin Nb_3Sn strands on the critical current and the magnetization losses. *Physica C*, 357–360:1289–1292, 2001.

[Fil02a] H. Fillunger, M. Foitl, K. Hense, I. Kajgana, A. Kasztler, H. Kirchmayr, R. Lackner, J. Leoni, R. Maix, T. Matthias, and J. Fidler.

Influence of the annealing time of internal tin Nb_3Sn strands on the critical current and the magnetization losses. *Physica C*, 372–376:1758–1761, 2002.

[Fil02b] H. Fillunger, M. Foitl, K. Hense, I. Kajgana, A. Kasztler, H. Kirchmayr, R. Lackner, J. Leoni, R. Maix, and M. Müller. Optimized heat treatment of internal tin Nb_3Sn strands. *IEEE Transactions on Applied Superconductivity*, 12(1):1049–1051, March 2002.

[Fis01] B. Fischer, T. Arndt, J. Gierl, H. Krauth, M. Munz, A. Szulczyk, M. Leghissa, and H.-W. Neumüller. Fabrication of Bi-2223 tapes. *IEEE Transactions on Applied Superconductivity*, 11(1):3261–3264, March 2001.

[Foi01] M. Foitl. Magnetisation and loss measurements on Nb_3Sn and NbTi strands for ITER and LHC. Ph.D. thesis, Technische Universität Wien, 2001.

[Fuj02] J. Fujikami, T. Kaneko, N. Ayai, S. Kobayashi, K. Hayashi, H. Takei, and K. Sato. Development of the industrial scale Ag/Bi-2223 tape. *Physica C*, 378-381:1061–1064, 2002.

[Göm97] F. Gömöry, L. Gherardi, R. Mele, D. Morin, and G. Crotti. Critical state and AC losses in multifilamentary BiSrCaCuO-2223/Ag tapes studied by transport and magnetic measurements. *Physica C*, 279:39–46, 1997.

[Gra97a] G. Grasso and R. Flükiger. Development of rectangular Bi-2223 wires with reduced anisotropy. *Superconductor Science and Technology*, 10:223–226, April 1997.

[Gra97b] G. Grasso, F. Marti, Y. Huang, A. Perin, and R. Flükiger. Correlation between the normal state resistivity and the critical current density of Ag sheathed Bi(2223) tapes. *Physica C*, 281:271–277, 1997.

[Han97] Z. Han, P. Skov-Hansen, and T. Freltoft. The mechanical deformation of superconducting BiSrCaCuO/Ag composites. *Superconductor Science and Technology*, 10:371–387, June 1997.

[Hen03] K. Hense, H. Fillunger, I. Kajgana, H. Kirchmayr, R. Lackner, R. K. Maix, and M. Müller. Optimisation of the reaction heat treatment cycle of internal tin and bronze Nb_3Sn strands for ITER. *Fusion Engineering and Design*, 66–68:1103–1107, 2003.

[Hua98] Y. B. Huang and R. Flükiger. Reducing ac losses of Bi(2223) multifilamentary tapes by oxide barriers. *Physica C*, 294:71–82, 1998.

[Inn04] Innova Superconductor Technology Co., Ltd. URL: http://www.innost.com, March 2004.

[ITE04] ITER Design Phase. URL: http://www.iter.org/ITERPublic/ITER/whatis.html, last updated: January 16^{th}, 2004.

[Kaj02] I. Kajgana. The optimisation of the heat treatment of Nb_3Sn strands and its influence on the RRR characteristics. Diploma thesis, Technische Universität Wien, 2002.

[Kan99] T. Kaneko, T. Hikata, M. Ueyama, A. Mikumo, N. Ayai, S. Kobayashi, N. Saga, K. Hayashi, K. Ohmatsu, and K. Sato. Status of Bi-2223 tapes performance and development. *IEEE Transactions on Applied Superconductivity*, 9(2):2465–2468, June 1999.

[Kel02] J. Kellers and L. J. Masur. Reliable commercial HTS wire for power applications. *Physica C*, 372-376:1040–1045, 2002.

[Kov95] P. Kováč, L. Cesnak, L. Kopera, H. Fikis, and G. Hilscher. I_c anisotropy in flattened Nb_3Sn superconductors and possible ways for overcoming it. *Cryogenics*, 35(2):83–86, 1995.

[Lar95] D. C. Larbalestier. Micro- and macro-structural factors which may control the superconducting properties of Nb_3Sn multifilamentary composite superconductors. *Cryogenics*, 35:15–18, 1995.

[Lee00] P. J. Lee, A. A. Squitieri, and D. C. Larbalestier. Nb_3Sn: macrostructure, microstructure and property comparisons for bronze and internal Sn process strands. *IEEE Transactions on Applied Superconductivity*, 10(1):979–982, March 2000.

[Mal99] A. P. Malozemoff, W. Carter, S. Fleshler, L. Fritzmeier, Q. Li, L. Masur, P. Miles, D. Parker, R. Parrella, E. Podtburg, G. N.

Riley, M. Rupich, J. Scudiere, and W. Zhang. HTS wires at commercial performance levels. *IEEE Transactions on Applied Superconductivity*, 9(2):2469–2473, June 1999.

[Mas01] L. Masur, D. Parker, M. Tanner, E. Podtburg, D. Buczek, J. Scudiere, P. Caracino, S. Spreafico, P. Corsaro, and M. Nassi. Long length manufacturing of BSCCO-2223 tape for the Detroit Edison power cable project. *IEEE Transactions on Applied Superconductivity*, 11(1):3256–3260, March 2001.

[OAW02] Controlled Thermonuclear Fusion – Euratom Associations. URL: http://europa.eu.int/comm/research/fusion/assoc.html, last updated: April 2nd 2002.

[Oom00] M. P. Oomen, J. Rieger, M. Leghissa, J. J. Rabbers, and B. ten Haken. The onset of full coupling in multi-filament superconducting tapes exposed to an alternating external magnetic field. *Physica C*, 340:87–92, 2000.

[Pol97] M. Polak, W. Zhang, X. Y. Cai, A. Polanskii, E. E. Hellstrom, D. C. Larbalestier, and M. Majoros. Current transfer lengths and the origin of linear components in the voltage-current curves of Ag-sheathed BSCCO components. *Superconductor Science and Technology*, 10:769–777, October 1997.

[Pol01] A. Polyanskii, D. M. Feldmann, S. Patnaik, J. Jiang, X. Cai, D. Larbalestier, K. DeMoranville, D. Yu, and R. Parrella. Examination of current limiting mechanisms in monocore $Bi_2Sr_2Ca_2Cu_3O_x$ tape with high critical current density. *IEEE Transactions on Applied Superconductivity*, 11(1):3269–3272, March 2001.

[Ros78] A. C. Rose-Innes and E. H. Rhoderick. Introduction to superconductivity, volume 6 of *International Series in Solid State Physics*. Pergamon Press, second edition, 1978.

[Sch81] W. Schelb. Electron microscopic examination of multifilamentary bronze-processed Nb_3Sn. *Journal of Materials Science*, 16:2575, 1981.

[Shi98] A. Shikov, A. Nikulin, A. Silaev, A. Vorobieva, V. Pantsyrnyi, G. Vedernikov, N. Salunin, and S. Sudiev. Development of the superconductors for ITER magnet system. *Journal of Nuclear Materials*, 258–263:1929–1934, 1998.

[Sug97] M. Sugimoto, A. Kimura, M. Mimura, Y. Tanaka, H. Ishii, S. Honjo, and Y. Iwata. Electromagnetic interfilament coupling of silver-sheathed Bi-2223 multifilamentary tapes in transverse AC magnetic fields. *Physica C*, 279:225–232, 1997.

[Sum91] L. T. Summers, M. W. Guinan, J. R. Miller, and P. A. Hahn. A model for the prediction of Nb_3Sn critical current as a function of field, temperature, strain, and radiation damage. *IEEE Transactions on Magnetics*, 27(2):2041–2044, March 1991.

[Syt99] V. E. Sytnikov, A. V. Taran, V. A. Mitrokhin, A. V. Rychagov, O. G. Filatov, and S. A. Egorov. The long-length line for jacketing cable-in-conduit conductors. *Fusion Engineering and Design*, 45:209–216, 1999.

[Thu97] T. R. Thurston, P. Haldar, Y. L. Wang, M. Suenaga, N. M. Jisrawi, and U. Wildgruber. In *situ* measurements of texture and phase development in $(Bi, Pb)_2Sr_2Ca_2Cu_3O_{10}$–Ag tapes. *Journal of Materials Research*, 12(4):891–905, 1997.

[Tsu01] H. Tsuji, S. Egorov, J. Minervini, N. Mitchell, K. Okuno, and E. Salpietro. ITER R&D: Magnets: Conductor and Joint Development. *Fusion Engineering and Design*, 55:141–151, 2001.

[War86] W. H. Warnes and D. C. Larbalestier. Critical current distributions in superconducting composites. *Cryogenics*, 26:643–653, December 1986.

[Web79] H. W. Weber and O. Hittmair. Supraleitung. 64. Thiemig Taschenbücher, München, 1979.

[Yam01] K. Yamashita, F. Sumiyoshi, and H. Hayashi. Measurement of transport-current distribution and loss reduction in superconducting wires with transposed Bi-2223 filaments. *Physica C*, 357-360:1218–1221, 2001.

Curriculum vitae

Name	Dipl.-Ing. Martin MÜLLER
July 3^{rd}, 1976	Born in Vienna, Austria. Father: Ing. Friedrich MÜLLER, * April 11^{th}, 1931, technical employee. Mother: Irma MÜLLER nee FAIKL, * February 9^{th}, 1944, housewife.
1982 – 1986	Elementary school in Vienna (1100 WIEN, Bernhardtstalgasse 19).
1986 – 1994	Realgymnasium (BRG X, Laaer-Berg-Straße 1) in Vienna.
May 31^{st}, 1994	Matura passed with distinction.
January 2^{nd}, 1995 – August 31^{st}, 1995	National service (1. GdKp/GdB and StbKp/AFMB).
1995 – 2001	Study of Technical Physics at Vienna University of Technology.
October 1997 – June 2001	Tutor in the following exercise courses: "Arbeitsgemeinschaft Physik-Rechenübungen I and II", "Arbeitsgemeinschaft Rechenübungen Thermodynamik", "Arbeitsgemeinschaft Rechenübungen Quantenphysik", and "Laborübungen I, II, and III".
January 26^{th}, 1998	First diploma exam passed.
October 17^{th}, 2001	Second diploma exam passed. (Diploma work: "Aufbau eines Hochtemperatur-Mößbauer-Meßplatzes").
November 5^{th}, 2001	Obtained the degree Master of Science (Diplom-Ingenieur).

October 2001 – January 2003	University teaching positions for the exercise courses "Arbeitsgemeinschaft Physik-Rechenübungen I and II", "Arbeitsgemeinschaft Rechenübungen Thermodynamik", and "Arbeitsgemeinschaft Rechenübungen Quantenphysik".
Since July 2001	Scientific assistant of the Association EURATOM-ÖAW (Austrian Academy of Sciences) in the Institute of Solid State Physics at Vienna University of Technology; main research: superconductivity.